EPJ manuscript No.
(will be inserted by the editor)

Ratios of Helicity Amplitudes for Exclusive ρ^0 Electroproduction

The HERMES Collaboration

A. Airapetian,[12,15] N. Akopov,[26] Z. Akopov,[5] E.C. Aschenauer,[6,a] W. Augustyniak,[25] R. Avakian,[26] A. Avetissian,[26] E. Avetisyan,[5] S. Belostotski,[18] N. Bianchi,[10] H.P. Blok,[17,24] A. Borissov,[5,b] J. Bowles,[13] V. Bryzgalov,[19] J. Burns,[13] M. Capiluppi,[9] G.P. Capitani,[10] E. Cisbani,[21] G. Ciullo,[9] M. Contalbrigo,[9] P.F. Dalpiaz,[9] W. Deconinck,[5] R. De Leo,[2] L. De Nardo,[11,5] E. De Sanctis,[10] M. Diefenthaler,[14,8] P. Di Nezza,[10] M. Düren,[12] M. Ehrenfried,[12] G. Elbakian,[26] F. Ellinghaus,[4] R. Fabbri,[6] A. Fantoni,[10] L. Felawka,[22] S. Frullani,[21] D. Gabbert,[6] G. Gapienko,[19] V. Gapienko,[19] F. Garibaldi,[21] G. Gavrilov,[5,18,22] V. Gharibyan,[26] F. Giordano,[5,9] S. Gliske,[15] M. Golembiovskaya,[6] C. Hadjidakis,[10] M. Hartig,[5] D. Hasch,[10] G. Hill,[13] A. Hillenbrand,[6] M. Hoek,[13] Y. Holler,[5] I. Hristova,[6] Y. Imazu,[23] A. Ivanilov,[19] H.E. Jackson,[1] H.S. Jo,[11] S. Joosten,[14] R. Kaiser,[13,c] G. Karyan,[26] T. Keri,[12] E. Kinney,[4] A. Kisselev,[18] N. Kobayashi,[23] V. Korotkov,[19] V. Kozlov,[16] P. Kravchenko,[18] V.G. Krivokhijine,[7] L. Lagamba,[2] R. Lamb,[14] L. Lapikás,[17] I. Lehmann,[13] P. Lenisa,[9] L.A. Linden-Levy,[14] A. López Ruiz,[11] W. Lorenzon,[15] X.-G. Lu,[6] X.-R. Lu,[23] B.-Q. Ma,[3] D. Mahon,[13] N.C.R. Makins,[14] S.I. Manaenkov,[18] L. Manfré,[21] Y. Mao,[3] B. Marianski,[25] A. Martinez de la Ossa,[4] H. Marukyan,[26] C.A. Miller,[22] Y. Miyachi,[23] A. Movsisyan,[26] V. Muccifora,[10] M. Murray,[13] A. Mussgiller,[5,8] E. Nappi,[2] Y. Naryshkin,[18] A. Nass,[8] M. Negodaev,[6] W.-D. Nowak,[6] L.L. Pappalardo,[9] R. Perez-Benito,[12] N. Pickert,[8] P.E. Reimer,[1] A.R. Reolon,[10] C. Riedl,[6] K. Rith,[8] G. Rosner,[13] A. Rostomyan,[5] J. Rubin,[14] D. Ryckbosch,[11] Y. Salomatin,[19] F. Sanftl,[20] A. Schäfer,[20] G. Schnell,[6,11] K.P. Schüler,[5] B. Seitz,[13] T.-A. Shibata,[23] V. Shutov,[7] M. Stancari,[9] M. Statera,[9] E. Steffens,[8] J.J.M. Steijger,[17] F. Stinzing,[8] S. Taroian,[26] A. Terkulov,[16] A. Trzcinski,[25] M. Tytgat,[11] A. Vandenbroucke,[11] Y. Van Haarlem,[11] C. Van Hulse,[11] D. Veretennikov,[18] V. Vikhrov,[18] I. Vilardi,[2] S. Wang,[3] S. Yaschenko,[6,8] S. Yen,[22] W. Yu,[12] B. Zihlmann,[5] P. Zupranski[25]

[1]Physics Division, Argonne National Laboratory, Argonne, Illinois 60439-4843, USA
[2]Istituto Nazionale di Fisica Nucleare, Sezione di Bari, 70124 Bari, Italy
[3]School of Physics, Peking University, Beijing 100871, China
[4]Nuclear Physics Laboratory, University of Colorado, Boulder, Colorado 80309-0390, USA
[5]DESY, 22603 Hamburg, Germany
[6]DESY, 15738 Zeuthen, Germany
[7]Joint Institute for Nuclear Research, 141980 Dubna, Russia
[8]Physikalisches Institut, Universität Erlangen-Nürnberg, 91058 Erlangen, Germany
[9]Istituto Nazionale di Fisica Nucleare, Sezione di Ferrara and Dipartimento di Fisica, Università di Ferrara, 44100 Ferrara, Italy
[10]Istituto Nazionale di Fisica Nucleare, Laboratori Nazionali di Frascati, 00044 Frascati, Italy
[11]Department of Subatomic and Radiation Physics, University of Gent, 9000 Gent, Belgium
[12]Physikalisches Institut, Universität Gießen, 35392 Gießen, Germany
[13]SUPA, School of Physics and Astronomy, University of Glasgow, Glasgow G12 8QQ, United Kingdom
[14]Department of Physics, University of Illinois, Urbana, Illinois 61801-3080, USA
[15]Randall Laboratory of Physics, University of Michigan, Ann Arbor, Michigan 48109-1040, USA
[16]Lebedev Physical Institute, 117924 Moscow, Russia
[17]National Institute for Subatomic Physics (Nikhef), 1009 DB Amsterdam, The Netherlands
[18]Petersburg Nuclear Physics Institute, Gatchina, 188300 Leningrad region, Russia
[19]Institute for High Energy Physics, Protvino, 142281 Moscow region, Russia
[20]Institut für Theoretische Physik, Universität Regensburg, 93040 Regensburg, Germany
[21]Istituto Nazionale di Fisica Nucleare, Sezione Roma 1, Gruppo Sanità and Physics Laboratory, Istituto Superiore di Sanità, 00161 Roma, Italy
[22]TRIUMF, Vancouver, British Columbia V6T 2A3, Canada
[23]Department of Physics, Tokyo Institute of Technology, Tokyo 152, Japan
[24]Department of Physics and Astronomy, VU University, 1081 HV Amsterdam, The Netherlands

[a] Now at: Brookhaven National Laboratory, Upton, New York 11772-5000, USA
[b] Now at: Department of Physics and Astronomy 666 W.Hancock, Wayne State University, Detroit MI 48201, USA
[c] Present address: International Atomic Energy Agency, A-1400 Vienna, Austria

arXiv:1012.3676v2 [hep-ex] 2 May 2011

[25]Andrzej Soltan Institute for Nuclear Studies, 00-689 Warsaw, Poland
[26]Yerevan Physics Institute, 375036 Yerevan, Armenia

Received: May 3, 2011/ Revised version:

Abstract. Exclusive ρ^0-meson electroproduction is studied in the HERMES experiment, using a 27.6 GeV longitudinally polarized electron/positron beam and unpolarized hydrogen and deuterium targets in the kinematic region 0.5 GeV^2 $< Q^2 <$ 7.0 GeV^2, 3.0 GeV $< W <$ 6.3 GeV, and $-t' <$ 0.4 GeV^2. Real and imaginary parts of the ratios of the natural-parity-exchange helicity amplitudes T_{11} ($\gamma_T^* \to \rho_T$), T_{01} ($\gamma_T^* \to \rho_L$), T_{10} ($\gamma_L^* \to \rho_T$), and T_{1-1} ($\gamma_{-T}^* \to \rho_T$) to T_{00} ($\gamma_L^* \to \rho_L$) are extracted from the data. For the unnatural-parity-exchange amplitude U_{11}, the ratio $|U_{11}/T_{00}|$ is obtained. The Q^2 and t' dependences of these ratios are presented and compared with perturbative QCD predictions.

1 Introduction

Exclusive electroproduction of vector mesons, $e + N \rightarrow e' + V + N'$, has been the focus of investigation for decades. Not only is the reaction mechanism of intrinsic interest, but this process also offers the possibility of studying, in a model-dependent way, the structure of hadrons involved in the process [1,2]. Using the one-photon-exchange approximation, all the measurable observables in electroproduction can be expressed in terms of the virtual photon spin-density matrix and the helicity amplitudes $F_{\lambda_V \lambda'_N \lambda_\gamma \lambda_N}$ of the process

$$\gamma^*(\lambda_\gamma) + N(\lambda_N) \rightarrow V(\lambda_V) + N'(\lambda'_N) \; . \qquad (1)$$

Here, γ^* denotes the virtual photon exchanged between the lepton and the target nucleon, V denotes the produced vector meson, and $N(N')$ the initial (final) nucleon. The helicities of the particles are given in parentheses in Eq. (1). The helicity amplitudes are defined in the virtual-photon-nucleon center-of-mass (CM) system. In order to make the discussion of the transition $\gamma^* \rightarrow V$ more transparent, we shall henceforth often omit the nucleon helicity indices using the notation $F_{\lambda_V \lambda_\gamma}$ instead of $F_{\lambda_V \lambda'_N \lambda_\gamma \lambda_N}$. The properties of helicity amplitudes can be studied in detail because the spin-density matrix of the virtual photon is well known from quantum electrodynamics and the spin-density matrix of the produced vector meson is experimentally accessible.

For unpolarized targets, the formalism of the spin-density matrix elements (SDMEs) of the produced vector meson was first presented in Ref. [3], where expressions of SDMEs in terms of helicity amplitudes were established. The formalism was then extended to the case of polarized targets in Ref. [4]. Recently, a new general formalism for the description of the process in Eq. (1) through SDMEs was presented in Ref. [5].

In order to determine SDMEs from experimental data, the SDMEs are considered as being independent free parameters in the fitting of the production and decay angular distribution of the vector meson. This is referred to as the "SDME method" in the rest of this work.

SDMEs are dimensionless quantities and therefore depend on ratios of amplitudes rather than on amplitudes themselves. The exact expressions for SDMEs given in Refs. [3,4,5] can be rewritten in terms of amplitude ratios. In an alternative method of fitting the angular distribution, these ratios are considered as being independent free parameters. This method is referred to as the "amplitude method" in the rest of this work.

In order to extract the helicity amplitudes themselves, experimental data on the differential cross section with respect to the Mandelstam t variable, $d\sigma/dt$ (which is proportional to the sum of squared moduli of all the amplitudes) are required in addition to the experimentally determined amplitude ratios. An analysis of these combined data would allow the extraction of the moduli of all amplitudes and of the phase differences between them with the common phase remaining undetermined. However, the requisite information on nucleon spin-flip amplitudes is not available for data taken with unpolarized targets.

Exclusive meson production in hard lepton scattering has been shown to offer the possibility of constraining generalized parton distributions (GPDs), which provide correlated information on transverse spatial and longitudinal momentum distributions of partons in the nucleon [6,7,8,9,10,11,12,13,14,15,16]. Vector-meson production amplitudes contain various linear combinations of process-independent GPDs for quarks of various flavors and gluons. Access to GPDs relies on the factorization property of the process amplitude, i.e., the amplitude can be written as convolution of "non-perturbative" GPDs with amplitudes of hard partonic subprocesses calculated within the framework of perturbative quantum chromodynamics (pQCD) and quantum electrodynamics.

The amplitudes $F_{0\frac{1}{2}0\pm\frac{1}{2}}$ are the most interesting because, only for these and quantities constructed from them, was factorization proven [17]. Factorization is not proven for the other amplitudes nor for SDMEs, which depend on all helicity amplitudes. The amplitudes $F_{0\frac{1}{2}0\pm\frac{1}{2}}$ correspond to the transition of a longitudinally polarized (L) virtual photon to a longitudinally polarized vector meson, $\gamma^*_L \rightarrow V_L$, and dominate at large photon virtuality Q^2. Nevertheless, an application of the "modified perturbative approach" [12,13] assumes that the factorization property also holds for the amplitudes F_{11} and F_{01}. The agreement found between certain calculated SDMEs and those extracted from HERMES [18], ZEUS [19], and H1 [20] data supports this assumption. The differential and total cross sections for longitudinal ρ^0-meson production by longitudinal photons are reasonably well described in the GPD-

based approach of Refs. [11,12,14,15,16] not only at the high energies of the HERA collider experiments [21,22, 23,24,25] but also at intermediate energies covered by the fixed-target experiments E665 [26], HERMES [27], and CLAS [28,29].

Amplitude ratios are useful not only as a tool for obtaining F_{00}. They can be used to study the general properties [5,30,31,32] of the vector-meson-production amplitudes at very small and very large values of Q^2 and t. They can also be used to test theoretical models. For these purposes, an amplitude ratio is more convenient than an SDME, which constitutes a more complicated object since any SDME depends on all the amplitude ratios. The amplitudes of the non-diagonal $\gamma^* \to V$ transitions F_{01} and F_{10} are known [31] to be zero if any valence quark in the vector meson carries half of the longitudinal momentum of the meson in the infinite momentum frame. These amplitudes are the most sensitive objects for the study of the quark motion in vector mesons. The double-spin-flip amplitude F_{1-1} contains information on the gluon transversity generalized parton distribution [9,10,30,31, 32,33] in the nucleon, which cannot be obtained from inclusive deep-inelastic lepton-nucleon scattering.

Amplitude ratios in ρ^0 and ϕ meson production on the proton were first studied by the H1 experiment [20] at the HERA collider. The results of the analysis of ρ^0-meson production at HERMES using the SDME method were published in Ref. [18], where also the description of the HERMES spectrometer and details of the data treatment etc. can be found. The present work is a continuation of that analysis. In the analysis presented in this paper, ratios of helicity amplitudes to the amplitude $F_{0\frac{1}{2}0\frac{1}{2}}$ are extracted separately for data taken with unpolarized hydrogen and deuterium targets first and then also for the combined datasets in a single analysis. A comparison of the proton and deuteron results allows the study of the degree of interference between $I = 1$ exchanges of $q\bar{q}$ pairs and $I = 0$ exchanges of $q\bar{q}$ pairs and two gluons.

2 Kinematics

In accordance with the notation of Ref. [18], the kinematic variables of the process

$$eN \to e'\gamma^* N \to e'\rho^o N' \to e'\pi^+\pi^- N' \tag{2}$$

are defined as follows. The four-momenta of the incident and outgoing leptons are denoted by k and k', the difference of which defines the four-momentum $q = k - k'$ of the virtual photon γ^*. In the target rest frame (which is also called the laboratory or lab frame in this work), ϑ is the scattering angle between the incident and outgoing leptons, the energies of the leptons are denoted by E and E'. The photon virtuality, given by

$$Q^2 = -q^2 = -(k - k')^2 \overset{lab}{\approx} 4\,E\,E'\sin^2\frac{\vartheta}{2}, \tag{3}$$

is positive in leptoproduction. In this equation, the electron rest mass is neglected. The four-momentum of the incident (recoiling) nucleon is denoted by p (p'). The Bjorken

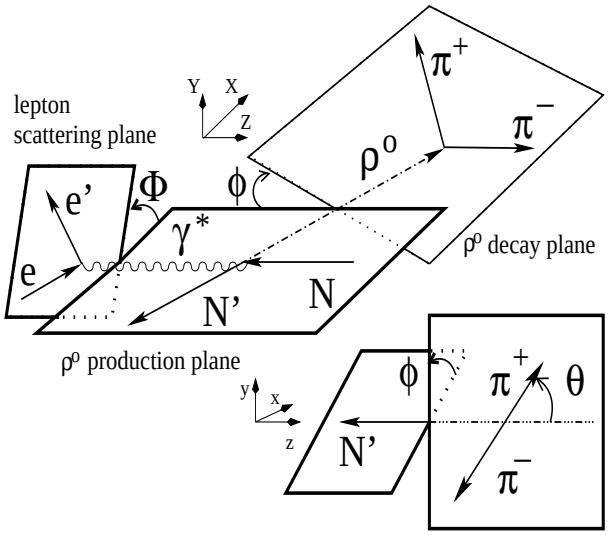

Fig. 1. Definition of angles in the process $eN \to e'\gamma^* N \to e'\rho^o N' \to e'\pi^+\pi^- N'$. Here Φ is the angle between the ρ^0 production plane and the lepton scattering plane in the CM system of virtual photon and target nucleon. See Ref. [34] for details. The variables θ and ϕ are respectively the polar and azimuthal angles of the decay π^+ in the ρ^0-meson rest frame, with the Z axis being anti-parallel to the outgoing nucleon momentum.

scaling variable x_B is defined as

$$x_B = \frac{Q^2}{2\,p\cdot q} = \frac{Q^2}{2\,M\,\nu}, \tag{4}$$

with

$$\nu = \frac{p\cdot q}{M} \overset{lab}{=} E - E', \tag{5}$$

so that ν represents the energy transfer from the incoming lepton to the virtual photon in the laboratory frame. The squared invariant mass of the photon-nucleon system is given by

$$W^2 = (p+q)^2 = M^2 + 2\,M\,\nu - Q^2. \tag{6}$$

The Mandelstam variable t is defined by the relation

$$t = (q - v)^2, \tag{7}$$

where v is the four-momentum of the ρ^0 meson being equal to $p_{\pi^+} + p_{\pi^-}$, the sum of π^+ and π^- four-momenta. The variables t, t_0, and $t' = t - t_0$ are always negative, where $-t_0$ is the minimal value of $-t$ for given values of Q^2, W, and the ρ^0-meson mass M_V. At small values of $-t'$, the approximation $-t' \approx v_T^2$ holds, where v_T is the transverse momentum of the ρ^0 meson with respect to the direction of the virtual photon in the CM system.

The variable ϵ represents the ratio of fluxes of longitudinally and transversely polarized virtual photons and is given by

$$\epsilon = \frac{1 - y - \frac{Q^2}{4E^2}}{1 - y + \frac{y^2}{2} + \frac{Q^2}{4E^2}} \overset{lab}{\approx} \left(1 + 2\left(1 + \frac{\nu^2}{Q^2}\right)\tan^2\frac{\vartheta}{2}\right)^{-1} \tag{8}$$

with $y = p \cdot q / p \cdot k \overset{lab}{=} \nu / E$.

The "exclusivity" of ρ^0 production in the process in Eq. (2) is characterized by the variable

$$\Delta E = \frac{M_X^2 - M^2}{2M} \overset{lab}{=} E_V - (E_{\pi^+} + E_{\pi^-}), \qquad (9)$$

where $M_X = \sqrt{(k - k' + p - p_{\pi^+} - p_{\pi^-})^2}$ is the reconstructed invariant mass of the undetected hadronic system (missing mass), $E_V = \nu + t/(2M)$ is the energy of the exclusively produced ρ^o meson, and $(E_{\pi^+} + E_{\pi^-})$ is the sum of the energies of the two detected pions in the laboratory system. For exclusive ρ^0 electroproduction $M_X = M$ and therefore $\Delta E = 0$.

The angles used for the description of the process in Eq. (2) are defined according to Ref. [34] (see also Ref. [18]) and presented in Fig. 1.

3 Formalism

3.1 Natural and Unnatural-Parity Exchange Helicity Amplitudes

In Ref. [3], exclusive ρ^0-meson leptoproduction is described by helicity amplitudes $F_{\lambda_V \lambda'_N \lambda_\gamma \lambda_N}$ defined in the right-handed CM system of the virtual photon and target nucleon. In this system, the Z-axis is aligned along the virtual photon three-momentum $\boldsymbol{q}$ and the Y-axis is parallel to $\boldsymbol{q} \times \boldsymbol{v}$ where $\boldsymbol{v}$ is the ρ^0 meson three-momentum as shown in Fig. 1. The helicity amplitude can be expressed as the scalar product of the matrix element of the electromagnetic current vector J^κ and the virtual-photon polarization vector $e_\kappa^{(\lambda_\gamma)}$

$$F_{\lambda_V \lambda'_N \lambda_\gamma \lambda_N} = (-1)^{\lambda_\gamma} \langle v \lambda_V p' \lambda'_N | J^\kappa | p \lambda_N \rangle e_\kappa^{(\lambda_\gamma)}, \qquad (10)$$

where a summation over the Lorentz index κ is performed. Here $e_\kappa^{(\pm 1)}$ and $e_\kappa^{(0)}$ indicate respectively transverse and longitudinal polarization of the virtual photon in the CM system:

$$e^{(\pm 1)} = (e_0, e_X, e_Y, e_Z) = (0, \mp\frac{1}{\sqrt{2}}, -\frac{i}{\sqrt{2}}, 0)\ , \qquad (11)$$

$$e^{(0)} = \frac{1}{Q}(q_Z, 0, 0, q_0) = \frac{1}{WQ}(M\sqrt{\nu^2 + Q^2}, 0, 0, M\nu - Q^2)\ . \qquad (12)$$

The ket vector $|p\lambda_N\rangle$ corresponds to the initial nucleon and the bra vector $\langle v\lambda_V p'\lambda'_N|$ represents the final state consisting of a ρ^0 meson and the scattered nucleon.

Any helicity amplitude $F_{\lambda_V \lambda'_N \lambda_\gamma \lambda_N}$ can be decomposed into the sum of an amplitude $T_{\lambda_V \lambda'_N \lambda_\gamma \lambda_N}$ for natural-parity exchange (NPE) and an amplitude $U_{\lambda_V \lambda'_N \lambda_\gamma \lambda_N}$ for unnatural-parity exchange (UPE) [3,4,5]

$$F_{\lambda_V \lambda'_N \lambda_\gamma \lambda_N} = T_{\lambda_V \lambda'_N \lambda_\gamma \lambda_N} + U_{\lambda_V \lambda'_N \lambda_\gamma \lambda_N}\,, \qquad (13)$$

which obey the following symmetry relations

$$T_{\lambda_V \lambda'_N \lambda_\gamma \lambda_N} = (-1)^{-\lambda_V + \lambda_\gamma} T_{-\lambda_V \lambda'_N - \lambda_\gamma \lambda_N} = (-1)^{\lambda'_N - \lambda_N} T_{\lambda_V - \lambda'_N \lambda_\gamma - \lambda_N}\,, \qquad (14)$$

$$U_{\lambda_V \lambda'_N \lambda_\gamma \lambda_N} = -(-1)^{-\lambda_V + \lambda_\gamma} U_{-\lambda_V \lambda'_N - \lambda_\gamma \lambda_N} = -(-1)^{\lambda'_N - \lambda_N} U_{\lambda_V - \lambda'_N \lambda_\gamma - \lambda_N}\ . \qquad (15)$$

There are three important consequences of the symmetry relations (14) and (15) [3,5]:
i) The number of linearly independent NPE amplitudes is equal to 10 while only 8 independent UPE amplitudes describe the process in Eq. (1),
ii) No UPE amplitude exists for the transition $\gamma_L \to \rho^0_L$, so that in particular $F_{0\frac{1}{2}0\frac{1}{2}} \equiv T_{0\frac{1}{2}0\frac{1}{2}} \equiv T_{00}$,
iii) For unpolarized targets there is no interference between NPE and UPE amplitudes [3,5].

In Regge phenomenology [35,36], an exchange of a single natural-parity reggeon [$P = (-1)^J$ (pomeron, secondary reggeons ρ, f_2, a_2, ...)] contributes to the NPE amplitudes, while an exchange of a single unnatural-parity reggeon [$P = -(-1)^J$ (π, a_1, b_1,...)] contributes to the UPE amplitudes [37]. It is worth noting that for a multi-reggeon-exchange contribution, there is no such one-to-one correspondence. For example, an exchange of two reggeons of "unnatural" parity contributes to the NPE amplitudes.

For convenience, we introduced in Ref. [18] the abbreviation $\widetilde{\sum} \equiv \frac{1}{2}\sum_{\lambda'_N \lambda_N}$ for the summation over the final nucleon helicity indices and for averaging over the initial spin states of the nucleon. For NPE amplitudes, transitions that are diagonal in nucleon helicity ($\lambda'_N = \lambda_N$) are dominant. In this case, neglecting the small nucleon helicity-flip amplitudes $T_{\lambda_V \pm \frac{1}{2} \lambda_\gamma \mp \frac{1}{2}}$ and using Eq. (14), the summation and averaging operation $\widetilde{\sum}$ reduces to one term:

$$\widetilde{\sum} T_{\lambda_V \lambda_\gamma} T^*_{\lambda'_V \lambda'_\gamma} \equiv \frac{1}{2} \sum_{\lambda_N \lambda'_N} T_{\lambda_V \lambda'_N \lambda_\gamma \lambda_N} T^*_{\lambda'_V \lambda'_N \lambda'_\gamma \lambda_N} = T_{\lambda_V \frac{1}{2} \lambda_\gamma \frac{1}{2}} T^*_{\lambda'_V \frac{1}{2} \lambda'_\gamma \frac{1}{2}} + T_{\lambda_V - \frac{1}{2} \lambda_\gamma \frac{1}{2}} T^*_{\lambda'_V - \frac{1}{2} \lambda'_\gamma \frac{1}{2}} \approx T_{\lambda_V \frac{1}{2} \lambda_\gamma \frac{1}{2}} T^*_{\lambda'_V \frac{1}{2} \lambda'_\gamma \frac{1}{2}} \equiv T_{\lambda_V \lambda_\gamma} T^*_{\lambda'_V \lambda'_\gamma}, \qquad (16)$$

where $T^*_{\lambda'_V \lambda'_N \lambda'_\gamma \lambda_N}$ represents the complex conjugate of the amplitude $T_{\lambda'_V \lambda'_N \lambda'_\gamma \lambda_N}$. Due to symmetry properties (see Eq. (14)), the abbreviated notation $T_{\lambda_V \lambda_\gamma}$ is used for the amplitudes $T_{\lambda_V \frac{1}{2} \lambda_\gamma \frac{1}{2}} = T_{\lambda_V - \frac{1}{2} \lambda_\gamma - \frac{1}{2}}$.

In general, no dominance for UPE amplitudes can be proven either for diagonal transitions ($\lambda_N = \lambda'_N$) or for transitions with nucleon helicity flip. Therefore, no relation analogous to Eq. (16) can be derived.

3.2 Spin Density Matrix Elements

The photon-spin-density matrix normalized to unit flux of transversely polarized virtual photons embodies the matrices $\varrho^U_{\lambda_\gamma \mu_\gamma}$ and $\varrho^L_{\lambda_\gamma \mu_\gamma}$ corresponding to unpolarized (U)

and longitudinally (L) polarized lepton beams:

$$\varrho^{U+L}_{\lambda_\gamma\mu_\gamma} = \varrho^{U}_{\lambda_\gamma\mu_\gamma} + P_B\ \varrho^{L}_{\lambda_\gamma\mu_\gamma}, \tag{17}$$

where P_B is the longitudinal polarization of the lepton beam and $\varrho^{U}_{\lambda_\gamma\mu_\gamma}$ and $\varrho^{L}_{\lambda_\gamma\mu_\gamma}$ are defined in Ref. [18]. The spin density matrix $\rho_{\lambda_V\mu_V}$ of the produced ρ^0 meson is related to that of the virtual photon, $\varrho^{U+L}_{\lambda_\gamma\mu_\gamma}$, through the von Neumann formula [3] :

$$\rho_{\lambda_V\mu_V} = \frac{1}{2\mathcal{N}} \sum_{\lambda_\gamma\mu_\gamma\lambda_N\lambda'_N} F_{\lambda_V\lambda'_N\lambda_\gamma\lambda_N}\ \varrho^{U+L}_{\lambda_\gamma\mu_\gamma}\ F^*_{\mu_V\lambda'_N\mu_\gamma\lambda_N}. \tag{18}$$

Note that the phase factor $(-1)^{\lambda_\gamma}$ in Eq. (10) is important for usual matrix summation over λ_γ and μ_γ in Eq. (18). The normalization factor is given by

$$\mathcal{N} = \mathcal{N}_T + \epsilon\mathcal{N}_L, \tag{19}$$

with

$$\mathcal{N}_T = \widetilde{\sum}\Big(|T_{11}|^2 + |T_{01}|^2 + |T_{1-1}|^2 + |U_{11}|^2 + |U_{01}|^2 + |U_{1-1}|^2\Big), \tag{20}$$

$$\mathcal{N}_L = \widetilde{\sum}\Big(|T_{00}|^2 + 2|T_{10}|^2 + 2|U_{10}|^2\Big). \tag{21}$$

Equation (21) is obtained by using the symmetry relations (14) and (15).

If the spin-density matrix of the virtual photon is decomposed into the standard set (see Ref. [3]) of nine hermitian matrices Σ^η ($\eta = 0,\ 1,\ ...,\ 8$), for the produced ρ^0 meson a set of nine matrices $r^\eta_{\lambda_V\mu_V}$ is obtained:

$$r^\eta_{\lambda_V\mu_V} = \frac{1}{2\mathcal{N}} \sum_{\lambda_\gamma\mu_\gamma\lambda'_N\lambda_N} F_{\lambda_V\lambda'_N\lambda_\gamma\lambda_N}\ \Sigma^\eta_{\lambda_\gamma\mu_\gamma}\ F^*_{\mu_V\lambda'_N\mu_\gamma\lambda_N}. \tag{22}$$

If an experiment is performed at fixed beam energy, a (Rosenbluth [38]) decomposition into contributions from longitudinally and transversely polarized virtual photons is impossible. In this case, the contributions from the matrix elements $r^0_{\lambda_V\mu_V}$ and $r^4_{\lambda_V\mu_V}$ cannot be disentangled and the only measurable combination is

$$r^{04}_{\lambda_V\mu_V} \equiv r^0_{\lambda_V\mu_V} + \epsilon r^4_{\lambda_V\mu_V}\ . \tag{23}$$

3.3 Three-dimensional Angular Distribution

The formula for the angular distribution of the scattered electrons/positrons and π^+ mesons from the decay $\rho^0 \to \pi^+\pi^-$ for the case of a longitudinally polarized beam and an unpolarized target [3] is given by

$$\mathcal{W}^{U+L}(\Phi,\phi,\cos\theta) = \mathcal{W}^{U}(\Phi,\phi,\cos\theta) + P_B\mathcal{W}^{L}(\Phi,\phi,\cos\theta)\ . \tag{24}$$

Here $\mathcal{W}^{U}(\Phi,\phi,\cos\theta)$ represents the angular distribution when both beam and target are unpolarized (see Eq. (25)) and $\mathcal{W}^{L}(\Phi,\phi,\cos\theta)$ is the additional term arising for longitudinally polarized beam (see Eq. (26)).

4 The Amplitude Method

4.1 Comparison of the SDME and Amplitude Methods

The SDME method for analyzing experimental data has the disadvantage that, in general, numerators of SDMEs depend on several ratios of helicity amplitudes (see Refs. [3, 18]) while the denominator common for all SDMEs depends on all the amplitude ratios. Therefore, if an SMDE extracted from data differs from model calculations, the source of the discrepancy is difficult to identify.

In total there are 18 independent amplitudes [3,4,5]. Since SDMEs depend on ratios of these complex amplitudes to F_{00}, any SDME comprises 34 real, independent functions. However, the number of SDMEs to be extracted from experimental data in polarized particle scattering is larger. For instance, there are 47 SDMEs when both beam and target are longitudinally polarized, while the angular distribution for longitudinal beam polarization and transverse target polarization depends on 71 SDMEs [5]. While the SDMEs can be completely expressed in terms of amplitude ratios, the fact that there are many more SDMEs than amplitude ratios implies that the SDMEs obey some relations. Due to the complicated inter-dependence on amplitude ratios, SDMEs cannot be considered as independent quantities and amplitude ratios can provide a more economical basis for fitting angular distributions of decay particles. This implies that the SDME values calculated from extracted amplitude ratios can be expected to be more accurate than those from direct SDME fits.

SDMEs calculated using the extracted helicity amplitude ratios may differ from those obtained with the SDME method. The SDMEs calculated from amplitude ratios are more constrained than those obtained by the SDME method. In general, any set of SDMEs obtained with the SDME method is physical only if it can be described in terms of amplitude ratios. Certain conditions, called positivity constraints, that must be satisfied by SDMEs in order to be expressed through amplitude ratios were considered in Ref. [5]. However, the full set of conditions that must be satisfied by SDMEs in order to be expressible in terms of helicity amplitude ratios is currently unknown.

4.2 Hierarchy of Helicity Amplitudes

The number of amplitude ratios to be extracted from data can be reduced if there exists a hierarchy for the moduli of helicity amplitudes. For large photon virtuality Q^2 and small $|t'|$, such a hierarchy among helicity amplitudes was predicted theoretically [30,31] and confirmed experimentally [24,18,39]. According to this hierarchy, there are a few significant amplitudes while the contributions of other amplitudes may be neglected within the present experimental accuracy. In a given kinematic region, the hierarchy of the amplitudes is governed by one or more "small kinematic parameters" that determine the contribution of various amplitudes to the process.

$$\mathcal{W}^U(\Phi,\phi,\cos\theta) = \frac{3}{8\pi^2}\Bigg[\frac{1}{2}(1-r^{04}_{00}) + \frac{1}{2}(3r^{04}_{00}-1)\cos^2\theta - \sqrt{2}\mathrm{Re}\{r^{04}_{10}\}\sin 2\theta\cos\phi - r^{04}_{1-1}\sin^2\theta\cos 2\phi$$
$$- \epsilon\cos 2\Phi\Big(r^1_{11}\sin^2\theta + r^1_{00}\cos^2\theta - \sqrt{2}\mathrm{Re}\{r^1_{10}\}\sin 2\theta\cos\phi - r^1_{1-1}\sin^2\theta\cos 2\phi\Big)$$
$$- \epsilon\sin 2\Phi\Big(\sqrt{2}\mathrm{Im}\{r^2_{10}\}\sin 2\theta\sin\phi + \mathrm{Im}\{r^2_{1-1}\}\sin^2\theta\sin 2\phi\Big)$$
$$+ \sqrt{2\epsilon(1+\epsilon)}\cos\Phi\Big(r^5_{11}\sin^2\theta + r^5_{00}\cos^2\theta - \sqrt{2}\mathrm{Re}\{r^5_{10}\}\sin 2\theta\cos\phi - r^5_{1-1}\sin^2\theta\cos 2\phi\Big)$$
$$+ \sqrt{2\epsilon(1+\epsilon)}\sin\Phi\Big(\sqrt{2}\mathrm{Im}\{r^6_{10}\}\sin 2\theta\sin\phi + \mathrm{Im}\{r^6_{1-1}\}\sin^2\theta\sin 2\phi\Big)\Bigg], \quad (25)$$

$$\mathcal{W}^L(\Phi,\phi,\cos\theta) = \frac{3}{8\pi^2}\Bigg[\sqrt{1-\epsilon^2}\Big(\sqrt{2}\mathrm{Im}\{r^3_{10}\}\sin 2\theta\sin\phi + \mathrm{Im}\{r^3_{1-1}\}\sin^2\theta\sin 2\phi\Big)$$
$$+ \sqrt{2\epsilon(1-\epsilon)}\cos\Phi\Big(\sqrt{2}\mathrm{Im}\{r^7_{10}\}\sin 2\theta\sin\phi + \mathrm{Im}\{r^7_{1-1}\}\sin^2\theta\sin 2\phi\Big)$$
$$+ \sqrt{2\epsilon(1-\epsilon)}\sin\Phi\Big(r^8_{11}\sin^2\theta + r^8_{00}\cos^2\theta - \sqrt{2}\mathrm{Re}\{r^8_{10}\}\sin 2\theta\cos\phi - r^8_{1-1}\sin^2\theta\cos 2\phi\Big)\Bigg]. \quad (26)$$

4.2.1 s-Channel Helicity Conservation

It was observed [1,2] that, at small $|t'|$, the amplitudes with a helicity flip in the transition $\gamma^* \to V$ ($\lambda_V \neq \lambda_\gamma$) are much smaller than those for diagonal transitions where the helicity of the vector meson is equal to that of the virtual photon ($\lambda_V = \lambda_\gamma$). This behavior is controlled by the small parameter

$$\alpha = \frac{\sqrt{-t'}}{M}, \quad (27)$$

where M is a typical hadronic mass, usually taken to be the nucleon mass. This dominance of the $\gamma^* \to V$ transition that is diagonal with respect to helicity is called the s-channel helicity conservation (SCHC) approximation. Furthermore, it was shown [40] that for small $|t'|$ and $Q^2 > 2M^2$, NPE amplitudes with nucleon helicity flip are suppressed compared to amplitudes describing diagonal transitions with $\lambda_N = \lambda'_N$. The same small parameter given by Eq. (27) controls this suppression.

As only an unpolarized target is considered here, there is no linear contribution of nucleon-helicity-flip amplitudes to the relevant SDMEs [3,5]. The fractional contribution of NPE amplitudes with nucleon helicity flip is suppressed by a factor α^2, so that we need to consider only NPE amplitudes with $\lambda_N = \lambda'_N$ if we neglect terms of order α^2.

The SCHC NPE amplitudes are T_{00} and T_{11}. The helicity-flip amplitudes T_{01} and T_{10} are proportional to the small factor α, while the double-helicity-flip amplitude T_{1-1} is proportional to α^2.

4.2.2 Twist decomposition

At asymptotically large photon virtuality, all amplitudes can be decomposed into power series of another small parameter

$$\beta = \frac{M_V}{Q}. \quad (28)$$

An expansion in β corresponds to the twist decomposition. A theoretical analysis in the framework of pQCD was performed [30,31] for the amplitudes of the process in Eq. (1). It was shown [17] that only the dominant amplitude T_{00} receives twist-2 contribution, while all other amplitudes contain only higher-twist contributions. The amplitudes T_{11}, T_{01}, T_{1-1} are suppressed by β while the amplitude T_{10} is suppressed by β^2. SCHC and the twist decomposition lead to the following hierarchy of NPE amplitudes at small $|t'|$ and large Q^2:

$$|T_{00}|^2 \gg |T_{11}|^2 \gg |T_{01}|^2 \gg |T_{10}|^2 \sim |T_{1-1}|^2 . \quad (29)$$

Such a hierarchy was observed in the HERA collider experiments [19,20,39,24].

4.2.3 Asymptotic Behavior of Amplitudes at High Energy

At high energy, a third small parameter can be defined:

$$\gamma = \frac{M}{W} . \quad (30)$$

The asymptotic behavior of amplitudes at large W and small $|t|$ was studied experimentally, providing information that led to the development of Regge phenomenology [35,36]. The fractional contribution of various amplitudes to SDMEs can be estimated by applying the formula for the amplitude of the exchange of a reggeon R at small $|t|$ and large W, $F \propto (W^2/M^2)^{\alpha_R(t)}$, where $\alpha_R(t)$ is the Regge trajectory (the spin of the exchanged reggeon). As a rough estimate, we assume that the pomeron intercept $\alpha_P(0) \approx 1$. Hence the amplitude of pomeron exchange is proportional to the factor W^2/M^2. Secondary reggeons with natural parity have $\alpha_R(0) \approx 0.5$ which results in $F \propto W/M$. Intercepts for reggeons with unnatural parity are negative in accordance with the results of a Regge phenomenology analysis [35,36] of experimental data on

soft scattering of hadrons. Therefore, the Regge factor is less than $(W^2/M^2)^0 = 1$. In QCD, exchanges of secondary reggeons and reggeons with unnatural parity correspond to quark-antiquark exchanges, while pomeron exchange corresponds to two-gluon exchange. In other words, the ratio of amplitudes of quark-antiquark exchanges with natural parity to the amplitude of pomeron exchange is proportional to the parameter γ, while the ratio of amplitudes of quark-antiquark exchanges with unnatural parity to the amplitude of pomeron exchange is proportional to γ^2. Since there is no interference between contributions of NPE and UPE amplitudes to SDMEs measured on unpolarized targets, the fractional contribution of UPE amplitudes is suppressed by a factor γ^4. This explains why only NPE amplitudes survive at HERA collider energies.

In the context of single-reggeon exchange, the isospin $I = 1$ reggeon (ρ, a_2, ...) contribution to the amplitude of vector-meson production on the proton is of opposite sign to that on the neutron. In contrast, the $I = 0$ reggeon (pomeron, ω, f_2, ...) contribution to the amplitude is of the same sign for both proton and neutron. Hence, the results on SDMEs and amplitude ratios should be different for proton and deuteron if $I = 1$ and $I = 0$ contributions to the amplitude interfere. By comparing proton and deuteron results, the fractional contribution of $I = 1$ reggeons to the extracted amplitude ratios can be estimated.

4.2.4 Hierarchy of Amplitudes in the Kinematic Region of HERMES

In the HERMES kinematic region, the parameter β is larger than 0.3 and the relative sizes of SDMEs measured in exclusive ρ^0 production can be explained by the following hierarchy [18]:

$$\begin{aligned} |T_{00}|^2 \sim |T_{11}|^2 \gg |U_{11}|^2 > |T_{01}|^2 \gg |T_{10}|^2 \\ \sim |T_{1-1}|^2 > |U_{01}|^2 \sim |U_{10}|^2 \sim |U_{1-1}|^2, \end{aligned} \quad (31)$$

with the two largest amplitudes being T_{00} and T_{11}. The abbreviated notation $U_{\lambda_V \lambda_\gamma}$, where

$$|U_{\lambda_V \lambda_\gamma}|^2 \equiv |U_{\lambda_V \frac{1}{2} \lambda_\gamma -\frac{1}{2}}|^2 + |U_{\lambda_V \frac{1}{2} \lambda_\gamma \frac{1}{2}}|^2 \quad (32)$$

was introduced because, for UPE amplitudes, it is impossible to prove the dominance of those without nucleon helicity flip over those with helicity flip, in contrast to the NPE amplitudes. As shown in Eq. (31), the moduli of all the UPE amplitudes except U_{11} are smaller than those of the NPE amplitudes. The numerical estimate $|U_{11}|^2/(|T_{11}|^2 + \epsilon|T_{00}|^2) \approx 0.11 \pm 0.04$ obtained in Ref. [18] shows that the modulus of $|U_{11}|$ is even larger than that of $|T_{01}|$ (and the result of the fit done in the present work confirms this result) and the contribution of $|U_{11}|$ to the SDMEs cannot be neglected. This contribution is suppressed by a factor γ^4 which is smaller than 0.01 in the HERMES kinematic region 3.0 GeV $\leq W \leq$ 6.5 GeV. If the UPE amplitude U_{11} is due to pion exchange, its contribution may be significant in the HERMES kinematic region because of the large pion-nucleon coupling constant $g_{\pi NN}$.

Contributions from small amplitudes can be appreciable if they are multiplied by the largest amplitudes T_{00} or T_{11} in the numerators of SDME formulas. As the small amplitudes T_{01}, T_{10}, and T_{1-1} are multiplied by the largest amplitudes (see Ref. [3] and Appendix A of Ref. [18]), five complex NPE amplitudes have to be considered in total, i.e. the four ratios T_{11}/T_{00}, T_{01}/T_{00}, T_{10}/T_{00}, and T_{1-1}/T_{00}. Concerning the ratio U_{11}/T_{00}, only $|U_{11}|/|T_{00}|$ can be determined as there is no interference between UPE and NPE amplitudes for the case of an unpolarized target. The contribution of all other UPE amplitudes can be neglected [18]. In total, there are nine independent free parameters to be determined when fitting the angular distribution using the amplitude method.

4.3 Basic Formulas of the Amplitude Method

The exact formulas for SDMEs expressed in terms of helicity amplitudes are presented in Appendix A of Ref. [18]. In order to rewrite SDMEs in terms of the ratios of significant helicity amplitudes, we neglect the contributions from NPE nucleon helicity-flip amplitudes (using Eq. (16)) and from all UPE amplitudes except U_{11}. Then, dividing both the numerators and the denominator in the exact formulas for SDMEs by $|T_{00}|^2$, we arrive at approximate expressions for SDMEs in terms of certain amplitude ratios:

$$r^{04}_{00} \simeq \{\epsilon + |t_{01}|^2\}/N\,, \quad (33)$$

$$\mathrm{Re}\{r^{04}_{10}\} \simeq \mathrm{Re}\{\epsilon t_{10} + \frac{1}{2} t_{01}(t_{11} - t_{1-1})^*\}/N\,, \quad (34)$$

$$r^{04}_{1-1} \simeq \mathrm{Re}\{-\epsilon|t_{10}|^2 + t_{1-1}t^*_{11}\}/N\,, \quad (35)$$

$$r^{1}_{11} \simeq \mathrm{Re}\{t_{1-1}t^*_{11}\}/N\,, \quad (36)$$

$$r^{1}_{00} \simeq -|t_{01}|^2/N\,, \quad (37)$$

$$\mathrm{Re}\{r^{1}_{10}\} \simeq \frac{1}{2}\mathrm{Re}\{-t_{01}(t_{11} - t_{1-1})^*\}/N\,, \quad (38)$$

$$r^{1}_{1-1} \simeq \frac{1}{2}\{|t_{11}|^2 + |t_{1-1}|^2 - |u_{11}|^2\}/N\,, \quad (39)$$

$$\mathrm{Im}\{r^{2}_{10}\} \simeq \frac{1}{2}\mathrm{Re}\{t_{01}(t_{11} + t_{1-1})^*\}/N\,, \quad (40)$$

$$\mathrm{Im}\{r^{2}_{1-1}\} \simeq \frac{1}{2}\{-|t_{11}|^2 + |t_{1-1}|^2 + |u_{11}|^2\}/N\,, \quad (41)$$

$$r^{5}_{11} \simeq \frac{1}{\sqrt{2}}\mathrm{Re}\{t_{10}(t_{11} - t_{1-1})^*\}/N\,, \quad (42)$$

$$r^{5}_{00} \simeq \sqrt{2}\mathrm{Re}\{t_{01}\}/N\,, \quad (43)$$

$$\mathrm{Re}\{r^{5}_{10}\} \simeq \frac{1}{\sqrt{8}}\mathrm{Re}\{2t_{10}t^*_{01} + (t_{11} - t_{1-1})\}/N\,, \quad (44)$$

$$r^{5}_{1-1} \simeq \frac{1}{\sqrt{2}}\mathrm{Re}\{-t_{10}(t_{11} - t_{1-1})^*\}/N\,, \quad (45)$$

$$\mathrm{Im}\{r^{6}_{10}\} \simeq -\frac{1}{\sqrt{8}}\mathrm{Re}\{t_{11} + t_{1-1}\}/N\,, \quad (46)$$

$$\mathrm{Im}\{r^{6}_{1-1}\} \simeq \frac{1}{\sqrt{2}}\mathrm{Re}\{t_{10}(t_{11} + t_{1-1})^*\}/N\,, \quad (47)$$

$$\mathrm{Im}\{r^3_{10}\} \simeq -\frac{1}{2}\mathrm{Im}\{t_{01}(t_{11}+t_{1-1})^*\}/N\,, \quad (48)$$

$$\mathrm{Im}\{r^3_{1-1}\} \simeq -\mathrm{Im}\{t_{1-1}t^*_{11}\}/N\,, \quad (49)$$

$$\mathrm{Im}\{r^7_{10}\} \simeq \frac{1}{\sqrt{8}}\mathrm{Im}\{t_{11}+t_{1-1}\}/N\,, \quad (50)$$

$$\mathrm{Im}\{r^7_{1-1}\} \simeq \frac{1}{\sqrt{2}}\mathrm{Im}\{t_{10}(t_{11}+t_{1-1})^*\}/N, \quad (51)$$

$$r^8_{11} \simeq -\frac{1}{\sqrt{2}}\mathrm{Im}\{t_{10}(t_{11}-t_{1-1})^*\}/N\,, \quad (52)$$

$$r^8_{00} \simeq \sqrt{2}\mathrm{Im}\{t_{01}\}/N\,, \quad (53)$$

$$\mathrm{Re}\{r^8_{10}\} \simeq \frac{1}{\sqrt{8}}\mathrm{Im}\{-2t_{10}t^*_{01}+t_{11}-t_{1-1}\}/N\,, \quad (54)$$

$$r^8_{1-1} \simeq \frac{1}{\sqrt{2}}\mathrm{Im}\{t_{10}(t_{11}-t_{1-1})^*\}/N \quad (55)$$

where the normalization factor $N = \mathcal{N}/|T_{00}|^2$ is defined in accordance with Eqs. (19)-(21) by

$$\begin{aligned} N &= N_T + \epsilon N_L, \\ N_T &\simeq |t_{11}|^2 + |t_{01}|^2 + |t_{1-1}|^2 + |u_{11}|^2, \\ N_L &\simeq 1 + 2|t_{10}|^2. \end{aligned} \quad (56)$$

Here $t_{\lambda_V\lambda_\gamma} \equiv T_{\lambda_V\lambda_\gamma}/T_{00}$ and $|u_{11}|^2 \equiv |U_{11}|^2/|T_{00}|^2$ with $|U_{11}|^2$ defined in Eq. (32). There are nine independent real functions in Eqs. (33-56), namely: $\mathrm{Re}(t_{11})$, $\mathrm{Im}(t_{11})$, $\mathrm{Re}(t_{01})$, $\mathrm{Im}(t_{01})$, $\mathrm{Re}(t_{10})$, $\mathrm{Im}(t_{10})$, $\mathrm{Re}(t_{1-1})$, $\mathrm{Im}(t_{1-1})$, and $|u_{11}|$. Equations (33-56) are the basis for the extraction of the helicity amplitude ratios from the measured angular distributions and also for the calculation of SDMEs from amplitude ratios (see Sec. 6.5).

5 The HERMES Experiment

A detailed description of the HERMES experiment at DESY can be found in Ref. [41]. The data analyzed in this paper were collected between the years 1996 and 2005. A longitudinally polarized positron or electron beam of 27.6 GeV was scattered from pure hydrogen or deuterium gas targets internal to the HERA lepton storage ring. The lepton beam was transversely polarized due to an asymmetry in the emission of synchrotron-radiation [42] in the field of the dipole magnets. The transverse beam polarization was transformed locally into longitudinal polarization at the interaction point by spin rotators located upstream and downstream of the HERMES apparatus. The helicity of the beam was typically reversed every two months. For both positive and negative beam helicities, the beam polarization was continuously measured by two Compton polarimeters [43,44]. The average beam polarization for the hydrogen (deuterium) data set was 0.45 (0.47) after requiring $0.15 < P_B < 0.8$ in the analysis process, and the fractional uncertainty of the beam polarization was 3.4% (2.0%) [43,44]. Some of the data were collected with longitudinally or transversely polarized targets. However, the time-averaged polarization of the polarized targets was negligible, while the rapid (60-180s) reversal of the polarization direction minimized polarization bias due to detector effects.

HERMES was a forward spectrometer [41] in which both scattered lepton and produced hadrons were detected within an angular acceptance of ± 170 mrad horizontally, and $\pm(40-140)$ mrad vertically. The tracking system had a momentum resolution of about 1.5% and an angular resolution of about 1 mrad. Lepton identification was accomplished using a transition-radiation detector, a preshower scintillator counter, and the electromagnetic calorimeter. The particle identification system included a gas threshold Čerenkov counter, which was replaced in 1998 by a dual-radiator ring-imaging Čerenkov detector [45]. Combining the responses of these detectors in a likelihood method led to an average lepton identification efficiency of 98% with a hadron contamination of less than 1%. The event sample used in this analysis is exactly the same as that used in Ref. [18].

6 Extraction of Amplitude Ratios

The measurement of the angular distribution of the scattered electrons/positrons and the pions from the decay $\rho^0 \to \pi^+\pi^-$ is the basis for the extraction of spin density matrix elements $r^\eta_{\lambda_V\mu_V}$ in the SDME method and of helicity amplitude ratios $t_{\lambda_V\lambda_\gamma}$ and $|u_{11}|$ in the amplitude method. For a polarized lepton beam and an unpolarized target, the angular distribution of the pions is given by relations (24-26) in Sec. 3.3 (see also Refs. [3,18]), where the SDMEs are expressed in terms of helicity amplitude ratios according to Eqs. (33-56).

6.1 Binned Maximum Likelihood Method

Amplitude ratios are extracted with the same binned maximum likelihood method as in the previous SDME analysis (see Sec. 6 of Ref. [18]). In brief, the amplitude ratios in each of the kinematic bins are obtained by minimizing the difference between the 3-dimensional $(\cos\theta, \phi, \Phi)$ angular distribution of the experimental events and that of a sample of fully reconstructed Monte Carlo events. The latter are generated isotropically in $(\cos\theta, \phi, \Phi)$ using the rhoMC generator [47,48] for exclusive ρ^0 simulated in the instrumental context of the spectrometer, and passed through the same reconstruction chain as the experimental data. The generated Monte Carlo events are iteratively reweighted with the angular distribution given by Eqs. (24-26), with the amplitude ratios treated as free parameters.

The minimization itself and the uncertainty calculation are performed using the MINUIT package [49]. More details can be found in Ref. [18].

6.2 Results on Amplitude Ratios in Bins of Q^2 and $-t'$

Ratios of helicity amplitudes are extracted in a two-dimensional (Q^2, $-t'$) binning from the same HERMES proton

bin	$\langle Q^2\rangle$, GeV^2	$\langle -t'\rangle$, GeV^2	bin	$\langle Q^2\rangle$, GeV^2	$\langle -t'\rangle$, GeV^2
q_1t_1	0.817	0.019	q_3t_1	1.658	0.019
q_1t_2	0.823	0.068	q_3t_2	1.660	0.068
q_1t_3	0.821	0.146	q_3t_3	1.663	0.146
q_1t_4	0.815	0.280	q_3t_4	1.663	0.282
q_2t_1	1.184	0.019	q_4t_1	2.996	0.019
q_2t_2	1.188	0.068	q_4t_2	3.056	0.068
q_2t_3	1.189	0.145	q_4t_3	3.076	0.146
q_2t_4	1.188	0.282	q_4t_4	3.134	0.284

Table 1. Mean values of kinematic variables for 16 bins. The limits of the q_1, q_2, q_3, and q_4 bins for Q^2 are 0.5; 1.0; 1.4; 2.0; 7.0 GeV^2 while those of the t_1, t_2, t_3, and t_4 bins for $-t'$ are the following: 0.0; 0.04; 0.10; 0.20; 0.40 GeV^2.

and deuteron data sets as were used for the SDME analysis of Ref. [18]. The four Q^2 bins are denoted as q_1, q_2, q_3, and q_4 defined by the limits 0.5, 1.0, 1.4, 2.0, 7.0 GeV^2. The four $-t'$ bins are denoted as t_1, t_2, t_3, and t_4 defined by the limits 0.0, 0.04, 0.10, 0.20, 0.40 GeV^2. The mean values of Q^2 and $-t'$ in each bin are presented in Tab. 1. The results of the extraction of the amplitude ratios in 16 bins are presented in Tab. 2 for the proton data and in Tab. 3 for the deuteron data. In every (Q^2, $-t'$) bin, the nine free parameters are obtained from a fit to the 3-dimensional angular distribution without subtracting the background from semi-inclusive deep-inelastic scattering (SIDIS). The SIDIS background under the exclusive peak, i.e., in the region -1 GeV $< \Delta E < 0.6$ GeV, is estimated using the PYTHIA Monte Carlo generator [50] (see Ref. [18] for more details) and its effect is assigned as a systematic uncertainty.

6.3 Testing the Extraction Method

The self-consistency of the extraction of amplitude ratios is tested with rhoMC Monte Carlo data. The fit results obtained for the nine free parameters in several (Q^2, $-t'$) bins spanning the experimental kinematic range are used to calculate the 23 SDMEs according to Eqs. (33-56). These SDMEs are then used as input for a Monte Carlo simulation of the angular distribution described in Eqs. (24-26). This angular distribution is used to extract the nine free parameters again. The resulting amplitude ratios are found to be consistent with the input amplitude ratios within statistical uncertainties.

6.4 Systematic Uncertainties

In the extraction of SDMEs in Ref. [18], two main contributions to the total systematic uncertainty of the results were discussed. One was the uncertainty in the background contribution to the signal in the region of the exclusive peak in the ΔE distribution. The background was simulated with the PYTHIA Monte Carlo generator. In the present analysis, the amplitude ratios are determined with and without background subtraction. The systematic uncertainty due to the background is chosen to be the difference between the amplitude ratios of these two sets. The other main uncertainty arises from the reliance on Monte Carlo simulations to perform the extraction of amplitude ratios from data. There are uncertainties in the parameters of the description of ρ^0 production in the Monte Carlo that propagate through to the amplitude-ratio values presented in this paper. The parameterization of the total electroproduction cross section in rhoMC is chosen in the context of a vector-meson-dominance model [1] that incorporates a propagator-type Q^2 dependence, and also contains a Q^2 dependence of the ratio of the longitudinally-polarized virtual photon and the transversely-polarized virtual photon cross-sections. As the HERMES spectrometer acceptance depends on Q^2, different input parameters result in slightly different reconstructed isotropic angular distributions. The corresponding systematic uncertainty of the resulting helicity amplitude ratios is obtained by varying these parameters within one standard deviation in the total uncertainty of the parameters given in Refs. [27, 46, 47, 48]. The effect of a possible kinematic dependence of the t' slope of the cross section in the rhoMC generator is found to be negligible in the kinematic region of our experiment.

A third main contribution to the systematic uncertainty arises in the amplitude method as a result of the neglect of the small NPE nucleon helicity-flip amplitudes and all the UPE amplitudes except $U_{1\frac{1}{2}1\pm\frac{1}{2}}$. As shown in Appendix A, the real and imaginary parts of the deviation $\delta t_{\lambda_V\lambda_\gamma}$ and also $\delta|u_{11}|$ of the obtained amplitude ratios from the true values $t_{\lambda_V\lambda_\gamma}$ and $|u_{11}|$, respectively, can be estimated using the relations

$$|\delta\mathrm{Re}(t_{\lambda_V\lambda_\gamma})| = \frac{v_T^2}{2M^2}|t_{\lambda_V\lambda_\gamma}|, \tag{57}$$

$$|\delta\mathrm{Im}(t_{\lambda_V\lambda_\gamma})| = \frac{v_T^2}{2M^2}|t_{\lambda_V\lambda_\gamma}|, \tag{58}$$

$$\delta|u_{11}| = \frac{v_T^2}{8M^2}|u_{11}|. \tag{59}$$

These equations are used to calculate the systematic uncertainty for the amplitude method described in this paper.

Ratio	q_1t_1	q_1t_2	q_1t_3	q_1t_4
$\mathrm{Re}(t_{11})$	$0.975 \pm 0.121 \pm 0.297$	$0.961 \pm 0.101 \pm 0.213$	$1.363 \pm 0.140 \pm 0.309$	$1.037 \pm 0.176 \pm 0.230$
$\mathrm{Im}(t_{11})$	$0.542 \pm 0.187 \pm 0.052$	$0.285 \pm 0.145 \pm 0.174$	$0.082 \pm 0.285 \pm 0.104$	$0.783 \pm 0.147 \pm 0.213$
$\mathrm{Re}(t_{01})$	$0.025 \pm 0.044 \pm 0.056$	$0.112 \pm 0.036 \pm 0.047$	$0.214 \pm 0.064 \pm 0.050$	$0.182 \pm 0.048 \pm 0.116$
$\mathrm{Im}(t_{01})$	$-0.098 \pm 0170 \pm 0.211$	$0.111 \pm 0.111 \pm 0.136$	$0.315 \pm 0.120 \pm 0.073$	$0.107 \pm 0.108 \pm 0.107$
$\mathrm{Re}(t_{10})$	$0.037 \pm 0.038 \pm 0.050$	$-0.049 \pm 0.039 \pm 0.024$	$0.024 \pm 0.039 \pm 0.026$	$-0.010 \pm 0.056 \pm 0.043$
$\mathrm{Im}(t_{10})$	$-0.067 \pm 0.064 \pm 0.156$	$-0.066 \pm 0.068 \pm 0.009$	$0.005 \pm 0.069 \pm 0.023$	$0.050 \pm 0.067 \pm 0.021$
$\mathrm{Re}(t_{1-1})$	$-0.110 \pm 0.042 \pm 0.045$	$-0.021 \pm 0.037 \pm 0.079$	$-0.037 \pm 0.043 \pm 0.043$	$0.020 \pm 0.056 \pm 0.040$
$\mathrm{Im}(t_{1-1})$	$0.178 \pm 0.087 \pm 0.349$	$-0.147 \pm 0.092 \pm 0.055$	$-0.124 \pm 0.100 \pm 0.079$	$-0.172 \pm 0.079 \pm 0.104$
$\lvert u_{11}\rvert$	$0.329 \pm 0.070 \pm 0.021$	$0.424 \pm 0.049 \pm 0.032$	$0.391 \pm 0.063 \pm 0.124$	$0.357 \pm 0.077 \pm 0.070$
Ratio	q_2t_1	q_2t_2	q_2t_3	q_2t_4
$\mathrm{Re}(t_{11})$	$1.138 \pm 0.143 \pm 0.021$	$0.996 \pm 0.106 \pm 0.084$	$1.079 \pm 0.094 \pm 0.135$	$0.925 \pm 0.097 \pm 0.139$
$\mathrm{Im}(t_{11})$	$0.282 \pm 0.268 \pm 0.212$	$0.386 \pm 0.125 \pm 0.039$	$0.342 \pm 0.162 \pm 0.159$	$0.289 \pm 0.156 \pm 0.141$
$\mathrm{Re}(t_{01})$	$0.044 \pm 0.051 \pm 0.009$	$0.116 \pm 0.037 \pm 0.061$	$0.113 \pm 0.035 \pm 0.030$	$0.250 \pm 0.043 \pm 0.075$
$\mathrm{Im}(t_{01})$	$0.073 \pm 0.146 \pm 0.137$	$0.327 \pm 0.099 \pm 0.083$	$-0.009 \pm 0.141 \pm 0.069$	$0.265 \pm 0.107 \pm 0.055$
$\mathrm{Re}(t_{10})$	$0.001 \pm 0.054 \pm 0.011$	$-0.054 \pm 0.034 \pm 0.033$	$0.032 \pm 0.030 \pm 0.015$	$-0.065 \pm 0.032 \pm 0.020$
$\mathrm{Im}(t_{10})$	$-0.081 \pm 0.073 \pm 0.154$	$0.064 \pm 0.073 \pm 0.058$	$0.006 \pm 0.070 \pm 0.027$	$0.063 \pm 0.073 \pm 0.057$
$\mathrm{Re}(t_{1-1})$	$0.001 \pm 0.045 \pm 0.015$	$0.023 \pm 0.040 \pm 0.018$	$-0.017 \pm 0.036 \pm 0.021$	$-0.073 \pm 0.035 \pm 0.019$
$\mathrm{Im}(t_{1-1})$	$-0.041 \pm 0.137 \pm 0.271$	$0.002 \pm 0.078 \pm 0.019$	$-0.084 \pm 0.107 \pm 0.024$	$-0.099 \pm 0.069 \pm 0.034$
$\lvert u_{11}\rvert$	$0.499 \pm 0.040 \pm 0.039$	$0.429 \pm 0.042 \pm 0.081$	$0.418 \pm 0.046 \pm 0.119$	$0.359 \pm 0.055 \pm 0.055$
Ratio	q_3t_1	q_3t_2	q_3t_3	q_3t_4
$\mathrm{Re}(t_{11})$	$1.029 \pm 0.104 \pm 0.039$	$1.088 \pm 0.098 \pm 0.083$	$0.878 \pm 0.079 \pm 0.202$	$0.975 \pm 0.096 \pm 0.228$
$\mathrm{Im}(t_{11})$	$0.257 \pm 0.131 \pm 0.151$	$0.479 \pm 0.111 \pm 0.050$	$0.513 \pm 0.102 \pm 0.385$	$0.280 \pm 0.176 \pm 0.365$
$\mathrm{Re}(t_{01})$	$-0.052 \pm 0.039 \pm 0.052$	$0.008 \pm 0.032 \pm 0.060$	$0.113 \pm 0.035 \pm 0.081$	$0.194 \pm 0.044 \pm 0.064$
$\mathrm{Im}(t_{01})$	$0.357 \pm 0.127 \pm 0.480$	$0.100 \pm 0.100 \pm 0.004$	$0.123 \pm 0.092 \pm 0.275$	$-0.100 \pm 0.108 \pm 0.406$
$\mathrm{Re}(t_{10}0$	$0.074 \pm 0.028 \pm 0.021$	$0.043 \pm 0.028 \pm 0.011$	$-0.007 \pm 0.034 \pm 0.032$	$-0.032 \pm 0.038 \pm 0.036$
$\mathrm{Im}(t_{10})$	$-0.051 \pm 0.067 \pm 0.042$	$-0.129 \pm 0.058 \pm 0.031$	$0.075 \pm 0.053 \pm 0.173$	$0.025 \pm 0.113 \pm 0.120$
$\mathrm{Re}(t_{1-1})$	$-0.013 \pm 0.038 \pm 0.021$	$-0.019 \pm 0.035 \pm 0.037$	$0.034 \pm 0.037 \pm 0.101$	$-0.044 \pm 0.036 \pm 0.065$
$\mathrm{Im}(t_{1-1})$	$0.108 \pm 0.090 \pm 0.236$	$0.100 \pm 0.071 \pm 0.031$	$-0.186 \pm 0.071 \pm 0.071$	$0.037 \pm 0.098 \pm 0.185$
$\lvert u_{11}\rvert$	$0.423 \pm 0.055 \pm 0.048$	$0.323 \pm 0.068 \pm 0.084$	$0.346 \pm 0.056 \pm 0.085$	$0.445 \pm 0.050 \pm 0.191$
Ratio	q_4t_1	q_4t_2	q_4t_3	q_4t_4
$\mathrm{Re}(t_{11})$	$0.723 \pm 0.071 \pm 0.053$	$0.706 \pm 0.068 \pm 0.039$	$0.582 \pm 0.074 \pm 0.156$	$0.650 \pm 0.063 \pm 0.117$
$\mathrm{Im}(t_{11})$	$0.570 \pm 0.071 \pm 0.025$	$0.657 \pm 0.061 \pm 0.066$	$0.583 \pm 0.110 \pm 0.120$	$0.488 \pm 0.067 \pm 0.119$
$\mathrm{Re}(t_{01})$	$0.062 \pm 0.031 \pm 0.007$	$0.121 \pm 0.031 \pm 0.006$	$0.190 \pm 0.054 \pm 0.021$	$0.282 \pm 0.036 \pm 0.060$
$\mathrm{Im}(t_{01})$	$0.011 \pm 0.069 \pm 0.019$	$0.084 \pm 0.079 \pm 0.019$	$-0.129 \pm 0.0.57 \pm 0.154$	$-0.099 \pm 0.081 \pm 0.044$
$\mathrm{Re}(t_{10})$	$-0.013 \pm 0.030 \pm 0.011$	$-0.046 \pm 0.035 \pm 0.008$	$0.095 \pm 0.025 \pm 0.118$	$0.007 \pm 0.031 \pm 0.012$
$\mathrm{Im}(t_{10})$	$0.010 \pm 0.052 \pm 0.010$	$0.050 \pm 0.045 \pm 0.015$	$-0.181 \pm 0.060 \pm 0.258$	$0.003 \pm 0.044 \pm 0.058$
$\mathrm{Re}(t_{1-1})$	$0.000 \pm 0.034 \pm 0.007$	$0.065 \pm 0.034 \pm 0.007$	$0.027 \pm 0.040 \pm 0.033$	$0.024 \pm 0.031 \pm 0.011$
$\mathrm{Im}(t_{1-1})$	$0.029 \pm 0.056 \pm 0.005$	$-0.068 \pm 0.048 \pm 0.015$	$-0.038 \pm 0.040 \pm 0.142$	$-0.036 \pm 0.051 \pm 0.066$
$\lvert u_{11}\rvert$	$0.451 \pm 0.049 \pm 0.024$	$0.306 \pm 0.061 \pm 0.032$	$0.383 \pm 0.067 \pm 0.097$	$0.380 \pm 0.044 \pm 0.091$

Table 2. Ratios of helicity amplitudes in Q^2 and $-t'$ bins for proton data. The mean values of Q^2 and $-t'$ for all 16 bins are given in Tab. 1. The notations t_{kj} and $|u_{11}|$ are used for the amplitude ratios T_{kj}/T_{00} and $|U_{11}/T_{00}|$, respectively. The first uncertainties are statistical, the second are systematic.

The three main systematic uncertainties are added in quadrature to give the total systematic uncertainty presented in Tabs. 2 and 3.

The effect of radiative corrections onto the values of ρ^0 SDMEs extracted was shown to be negligible [18]. This is mainly due to the exclusivity cut $\Delta E < 0.6$ GeV that excludes photons radiated with more than 0.6 GeV. The amplitude ratios in this work are extracted using exactly the same data sets and cuts, by a very similar fit comparing the shapes of the 3-dimensional experimental and simulated angular distributions. Hence we conclude that

Ratio	q_1t_1	q_1t_2	q_1t_3	q_1t_4
$\mathrm{Re}(t_{11})$	$0.860 \pm 0.078 \pm 0.163$	$1.256 \pm 0.095 \pm 0.055$	$1.220 \pm 0.113 \pm 0.145$	$1.197 \pm 0.124 \pm 0.218$
$\mathrm{Im}(t_{11})$	$0.509 \pm 0.118 \pm 0.203$	$0.304 \pm 0.159 \pm 0.049$	$0.192 \pm 0.228 \pm 0.114$	$0.222 \pm 0.320 \pm 0.208$
$\mathrm{Re}(t_{01})$	$-0.011 \pm 0.029 \pm 0.027$	$0.020 \pm 0.032 \pm 0.069$	$0.174 \pm 0.044 \pm 0.080$	$0.151 \pm 0.052 \pm 0.042$
$\mathrm{Im}(t_{01})$	$0.023 \pm 0.076 \pm 0.070$	$0.088 \pm 0.076 \pm 0.035$	$0.239 \pm 0.112 \pm 0.086$	$0.222 \pm 0.143 \pm 0.164$
$\mathrm{Re}(t_{10})$	$-0.011 \pm 0.029 \pm 0.020$	$0.002 \pm 0.027 \pm 0.014$	$0.025 \pm 0.032 \pm 0.048$	$0.017 \pm 0.033 \pm 0.019$
$\mathrm{Im}(t_{10})$	$0.020 \pm 0.049 \pm 0.044$	$-0.017 \pm 0.063 \pm 0.047$	$-0.048 \pm 0.083 \pm 0.135$	$0.014 \pm 0.076 \pm 0.095$
$\mathrm{Re}(t_{1-1})$	$-0.017 \pm 0.029 \pm 0.018$	$0.056 \pm 0.030 \pm 0.051$	$-0.052 \pm 0.032 \pm 0.039$	$0.027 \pm 0.050 \pm 0.078$
$\mathrm{Im}(t_{1-1})$	$-0.062 \pm 0.064 \pm 0.020$	$-0.098 \pm 0.078 \pm 0.039$	$-0.093 \pm 0.093 \pm 0.153$	$-0.228 \pm 0.105 \pm 0.054$
$\lvert u_{11}\rvert$	$0.364 \pm 0.037 \pm 0.090$	$0.343 \pm 0.046 \pm 0.037$	$0.419 \pm 0.048 \pm 0.020$	$0.388 \pm 0.060 \pm 0.105$
Ratio	q_2t_1	q_2t_2	q_2t_3	q_2t_4
$\mathrm{Re}(t_{11})$	$0.984 \pm 0.087 \pm 0.048$	$0.888 \pm 0.080 \pm 0.126$	$1.119 \pm 0.074 \pm 0.129$	$0.990 \pm 0.063 \pm 0.140$
$\mathrm{Im}(t_{11})$	$0.341 \pm 0.106 \pm 0.054$	$0.778 \pm 0.078 \pm 0.153$	$0.252 \pm 0.105 \pm 0.163$	$0.039 \pm 0.142 \pm 0.482$
$\mathrm{Re}(t_{01})$	$0.042 \pm 0.023 \pm 0.022$	$0.071 \pm 0.028 \pm 0.028$	$0.109 \pm 0.025 \pm 0.037$	$0.262 \pm 0.031 \pm 0.043$
$\mathrm{Im}(t_{01})$	$0.289 \pm 0.130 \pm 0.084$	$-0.062 \pm 0.069 \pm 0.158$	$0.136 \pm 0.074 \pm 0.035$	$0.070 \pm 0.086 \pm 0.064$
$\mathrm{Re}(t_{10})$	$-0.006 \pm 0.027 \pm 0.020$	$0.039 \pm 0.025 \pm 0.038$	$0.039 \pm 0.019 \pm 0.012$	$0.022 \pm 0.029 \pm 0.048$
$\mathrm{Im}(t_{10})$	$0.029 \pm 0.101 \pm 0.052$	$-0.009 \pm 0.034 \pm 0.013$	$-0.087 \pm 0.044 \pm 0.007$	$-0.201 \pm 0.065 \pm 0.171$
$\mathrm{Re}(t_{1-1})$	$0.013 \pm 0.046 \pm 0.017$	$0.021 \pm 0.028 \pm 0.060$	$-0.077 \pm 0.007 \pm 0.012$	$-0.041 \pm 0.028 \pm 0.039$
$\mathrm{Im9}t_{1-1})$	$0.063 \pm 0.100 \pm 0.034$	$-0.042 \pm 0.046 \pm 0.042$	$0.030 \pm 0.070 \pm 0.012$	$-0.071 \pm 0.072 \pm 0.106$
$\lvert u_{11}\rvert$	$0.395 \pm 0.035 \pm 0.066$	$0.262 \pm 0.050 \pm 0.048$	$0.401 \pm 0.036 \pm 0.134$	$0.373 \pm 0.048 \pm 0.085$
Ratio	q_3t_1	q_3t_2	q_3t_3	q_3t_4
$\mathrm{Re}(t_{11})$	$0.787 \pm 0.059 \pm 0.052$	$0.819 \pm 0.065 \pm 0.067$	$0.839 \pm 0.076 \pm 0.076$	$0.835 \pm 0.060 \pm 0.128$
$\mathrm{Im}(t_{11})$	$0.487 \pm 0.072 \pm 0.081$	$0.518 \pm 0.085 \pm 0.079$	$0.553 \pm 0.088 \pm 0.111$	$0.203 \pm 0.097 \pm 0.129$
$\mathrm{Re}(t_{01})$	$0.028 \pm 0.024 \pm 0.030$	$0.094 \pm 0.025 \pm 0.053$	$0.129 \pm 0.028 \pm 0.017$	$0.222 \pm 0.028 \pm 0.034$
$\mathrm{Im}(t_{01})$	$0.102 \pm 0.080 \pm 0.021$	$0.001 \pm 0.091 \pm 0.042$	$-0.017 \pm 0.078 \pm 0.072$	$0.080 \pm 0.072 \pm 0.040$
$\mathrm{Re}(t_{10})$	$-0.006 \pm 0.024 \pm 0.003$	$-0.007 \pm 0.023 \pm 0.020$	$0.027 \pm 0.028 \pm 0.010$	$0.053 \pm 0.026 \pm 0.038$
$\mathrm{Im}(t_{10})$	$0.008 \pm 0.048 \pm 0.018$	$-0.025 \pm 0.045 \pm 0.042$	$-0.092 \pm 0.046 \pm 0.014$	$-0.228 \pm 0.058 \pm 0.035$
$\mathrm{Re}(t_{1-1})$	$0.031 \pm 0.026 \pm 0.026$	$-0.045 \pm 0.027 \pm 0.012$	$-0.018 \pm 0.032 \pm 0.052$	$-0.008 \pm 0.027 \pm 0.025$
$\mathrm{Im}(t_{1-1})$	$0.000 \pm 0.052 \pm 0.037$	$0.102 \pm 0.061 \pm 0.015$	$-0.038 \pm 0.065 \pm 0.048$	$-0.068 \pm 0.067 \pm 0.047$
$\lvert u_{11}\rvert$	$0.386 \pm 0.034 \pm 0.020$	$0.402 \pm 0.039 \pm 0.076$	$0.355 \pm 0.045 \pm 0.023$	$0.353 \pm 0.050 \pm 0.072$
Ratio	q_4t_1	q_4t_2	q_4t_3	q_4t_4
$\mathrm{Re}(t_{11})$	$0.655 \pm 0.054 \pm 0.044$	$0.842 \pm 0.068 \pm 0.043$	$0.768 \pm 0.060 \pm 0.079$	$0.820 \pm 0.075 \pm 0.315$
$\mathrm{Im}(t_{11})$	$0.629 \pm 0.049 \pm 0.011$	$0.614 \pm 0.066 \pm 0.052$	$0.592 \pm 0.059 \pm 0.089$	$0.614 \pm 0.070 \pm 0.273$
$\mathrm{Re}(t_{01})$	$0.060 \pm 0.025 \pm 0.003$	$0.147 \pm 0.030 \pm 0.010$	$0.144 \pm 0.029 \pm 0.018$	$0.243 \pm 0.031 \pm 0.105$
$\mathrm{Im}(t_{01})$	$-0.091 \pm 0.075 \pm 0.011$	$-0.065 \pm 0.067 \pm 0.018$	$-0.173 \pm 0.076 \pm 0.028$	$0.042 \pm 0.078 \pm 0.382$
$\mathrm{Re}(t_{10})$	$0.025 \pm 0.027 \pm 0.009$	$0.042 \pm 0.030 \pm 0.012$	$0.073 \pm 0.031 \pm 0.016$	$-0.014 \pm 0.034 \pm 0.063$
$\mathrm{Im}(t_{10})$	$-0.088 \pm 0.038 \pm 0.014$	$-0.148 \pm 0.047 \pm 0.010$	$-0.131 \pm 0.041 \pm 0.017$	$-0.025 \pm 0.049 \pm 0.043$
$\mathrm{Re}(t_{1-1})$	$-0.009 \pm 0.030 \pm 0.001$	$-0.004 \pm 0.032 \pm 0.017$	$-0.010 \pm 0.030 \pm 0.008$	$-0.009 \pm 0.030 \pm 0.046$
$\mathrm{Im}(t_{1-1})$	$0.016 \pm 0.038 \pm 0.006$	$-0.024 \pm 0.051 \pm 0.026$	$-0.050 \pm 0.042 \pm 0.075$	$-0.055 \pm 0.048 \pm 0.109$
$\lvert u_{11}\rvert$	$0.436 \pm 0.038 \pm 0.042$	$0.422 \pm 0.044 \pm 0.045$	$0.389 \pm 0.042 \pm 0.070$	$0.420 \pm 0.045 \pm 0.076$

Table 3. Ratios of helicity amplitudes in Q^2 and $-t'$ bins for deuteron data. The mean values of Q^2 and $-t'$ for all 16 bins are given in Tab. 1. The notations t_{kj} and $|u_{11}|$ are used for the amplitude ratios T_{kj}/T_{00} and $|U_{11}/T_{00}|$, respectively. The first uncertainties are statistical, the second are systematic.

any possible systematic uncertainty of amplitude ratios due to radiative corrections can be safely neglected.

6.5 Calculation of SDMEs from Extracted Helicity Amplitude Ratios

In the following, the SDME results obtained from SDME and amplitude methods are compared. The SDMEs are calculated for every (Q^2, $-t'$) bin by applying formu-

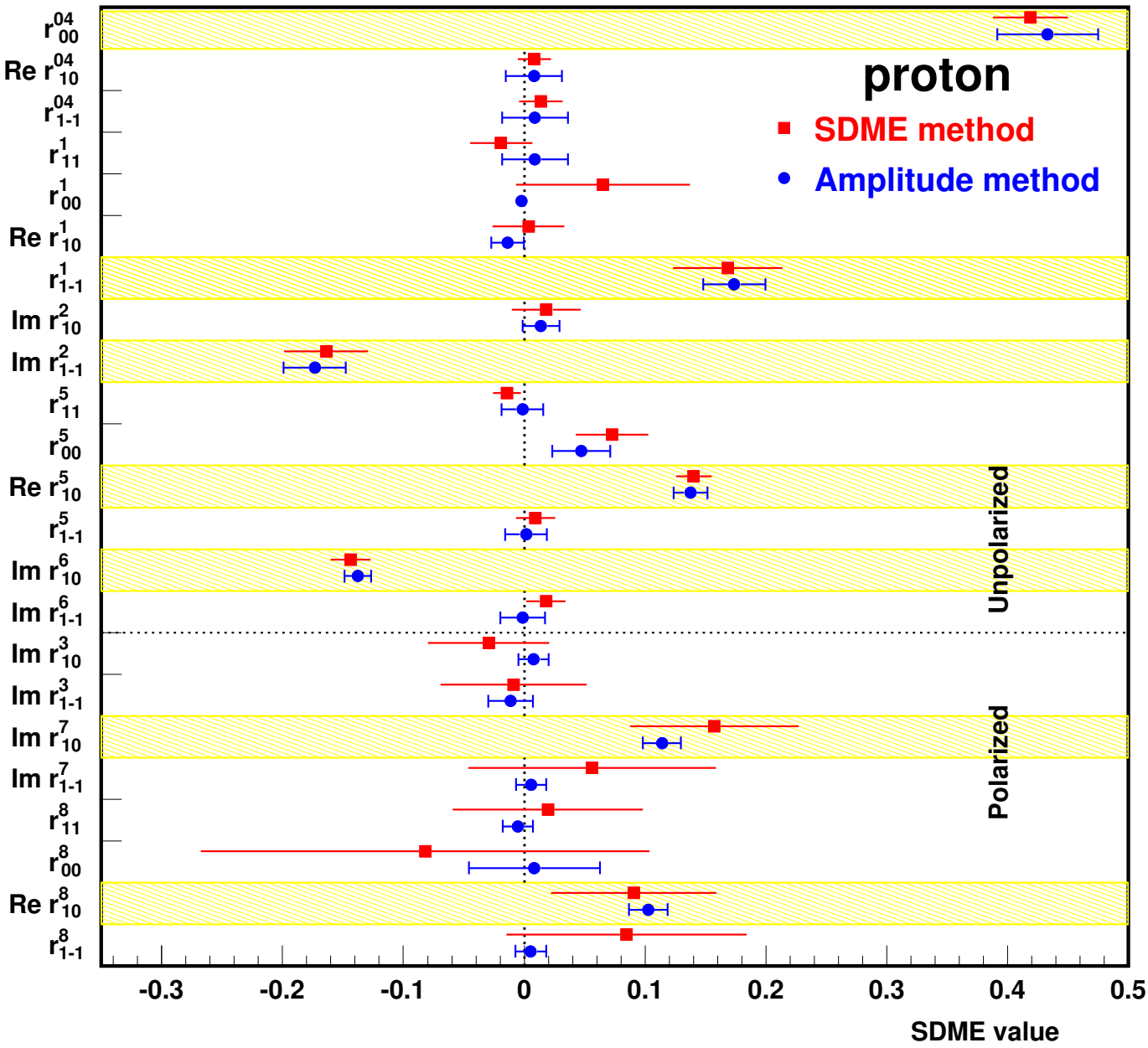

Fig. 2. Comparison of SDME and amplitude methods. Red squares show the results of the SDME analysis [18]. Blue circles (amplitude method) are obtained in the present work from amplitude ratios fitted directly to the three-dimensional angular distribution in every Q^2 and $-t'$ bin. The proton data at $\langle Q^2 \rangle = 3$ GeV^2, $\langle -t' \rangle = 0.019$ GeV^2 are presented. Yellow bands mark those SDMEs that are non-zero in the SCHC approximation. Total uncertainties are depicted.

las (33-56) and using the values of the real and imaginary parts of the amplitude ratios given in Tabs. 2 and 3. The results of both methods are found to agree over the full kinematic range of the experiment. The comparison is shown for two representative bins, for the proton data using the bin $q_4 t_1$ ($\langle Q^2 \rangle = 3$ GeV^2, $\langle -t' \rangle = 0.019$ GeV^2) in Fig. 2 and for deuteron data using the bin $q_2 t_3$ ($\langle Q^2 \rangle = 1.19$ GeV^2, $\langle -t' \rangle = 0.145$ GeV^2) in Fig. 3. The bands in the figures mark those SDMEs that may be non-zero in the SCHC approximation, while the line at zero is drawn for those SDMEs that vanish at $t' = 0$.

For the unpolarized SDMEs, the total uncertainties obtained with the amplitude method are in most cases comparable to those obtained with the SDME method. An exception seen in Fig. 2 is r^1_{00} which is proportional to $|t_{01}|^2$ (see Eq. (37)) and hence extremely small at small $|t'|$. For polarized SDMEs, the uncertainties obtained using the SDME method are generally much larger than those obtained using the amplitude method. This differ-

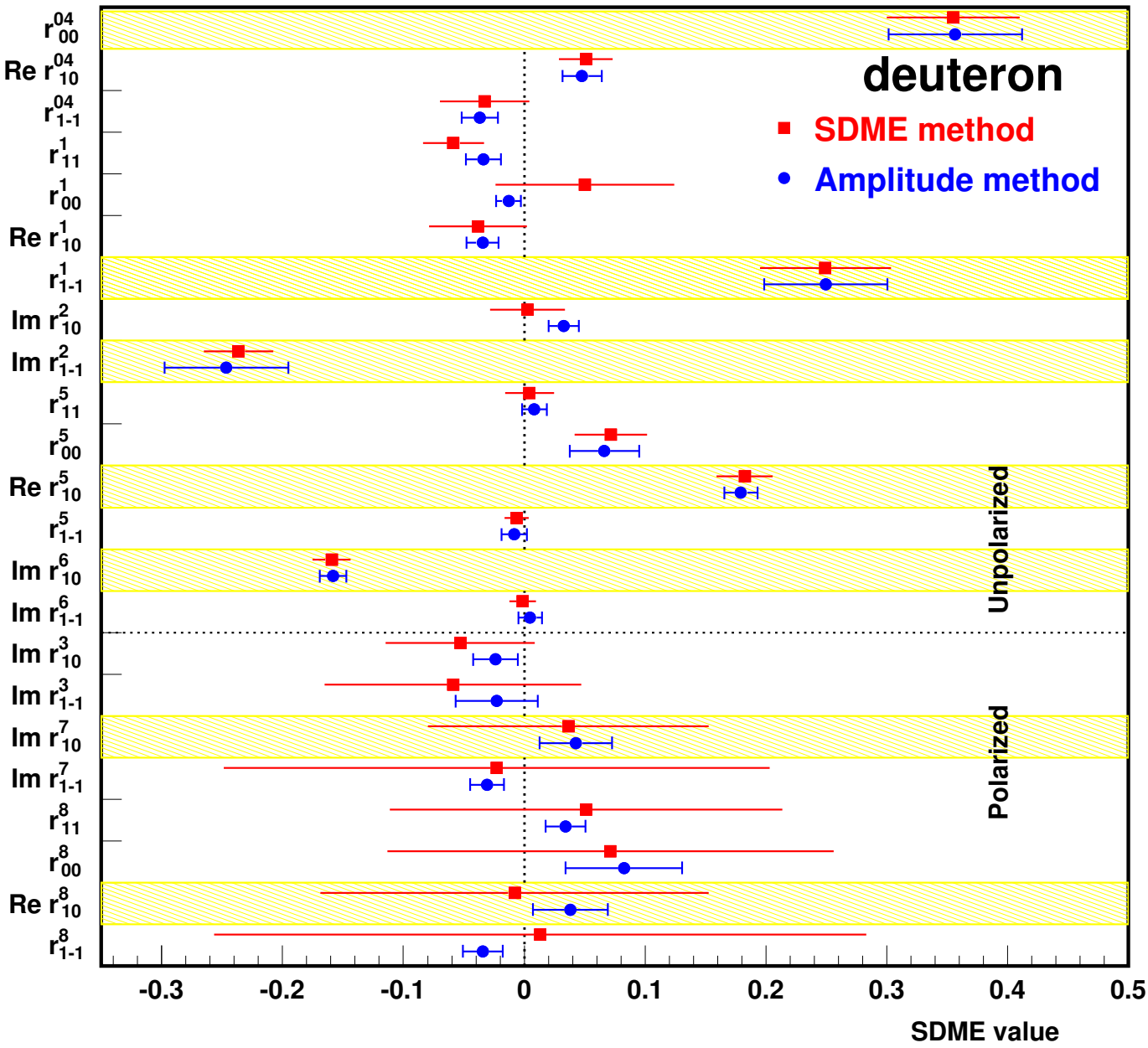

Fig. 3. Comparison of SDME and amplitude methods. Red squares show the results of the SDME analysis [18]. Blue circles (amplitude method) are obtained in the present work from amplitude ratios fitted directly to the three-dimensional angular distribution in every Q^2 and $-t'$ bin. The deuteron data at $\langle Q^2 \rangle = 1.19$ GeV^2, $\langle -t' \rangle = 0.145$ GeV^2 are presented. Yellow bands mark those SDMEs that are non-zero in the SCHC approximation. Total uncertainties are depicted.

ence reflects a major difference in the methods themselves. In the SDME method, polarized and unpolarized SDMEs are fitted as independent free parameters. In this case, the error bars of the polarized SDMEs are inflated due to the factors $P_B = 0.47$ and $\sqrt{1-\epsilon} \approx 0.45$ (see Eqs. (24-26)). However, Eqs. (33-56) show that the polarized SDMEs depend on amplitude ratios constrained by both polarized and unpolarized data. Hence the polarized SDMEs calculated from the amplitude ratios have uncertainties comparable to those of the unpolarized SDMEs. Nevertheless, the polarized data serves the important function of constraining the sign of the imaginary parts of amplitude ratios.

7 Kinematic Dependences of Amplitude Ratios

7.1 Predictions for Asymptotic Behavior

At small $|t'|$, the behavior of NPE amplitudes $T_{\lambda_V\lambda_\gamma}$ can be described [5] by

$$T_{\lambda_V\lambda_\gamma} \propto (-t')^{|\lambda_V-\lambda_\gamma|/2}, \tag{60}$$

which reflects angular momentum conservation in the process in Eq. (1). Equation (60) shows that T_{00} behaves as a constant at small $|t'|$. Hence each ratio $t_{\lambda_V\lambda_\gamma} = T_{\lambda_V\lambda_\gamma}/T_{00}$ has the same asymptotic behavior at $t' \to 0$ as the amplitude $T_{\lambda_V\lambda_\gamma}$.

The asymptotic behaviour of the amplitudes of vector-meson electroproduction at large Q^2 and small x_B was considered in Refs. [30,31] in the framework of pQCD, using the approximation of leading logarithms in which the logarithms $\ln(1/x_B)$ and $\ln(Q^2)$ are large, and the amplitudes are considered to be nearly imaginary. It was predicted [30,31,32] that the amplitude ratios should have the following behavior at large Q^2 and small x_B:

$$t_{11} \equiv T_{11}/T_{00} \propto \frac{M_V}{Q}, \tag{61}$$

$$t_{01} \equiv T_{01}/T_{00} \propto \frac{\sqrt{-t'}}{Q}, \tag{62}$$

$$t_{10} \equiv T_{10}/T_{00} \propto \frac{M_V\sqrt{-t'}}{Q^2+M_V^2}, \tag{63}$$

$$t_{1-1} \equiv T_{1-1}/T_{00} \propto \frac{-t'M_V}{Q}\left[\frac{C_1}{Q^2+M_V^2} + \frac{C_2}{\mu^2}\right]. \tag{64}$$

The functions C_1 and C_2 in Eq. (64) are dimensionless and the parameter μ is between 0.7 GeV and 1.0 GeV. It was noted in Refs. [30,31,32] that C_1 is essentially a constant while C_2 is a ratio whose numerator contains the gluon transversity distribution [33] $G_T(x_B,\mu^2)$ at the scale μ and the denominator contains the unpolarized gluon density $G(x_B,Q_V^2)$ measured at the conjectured [31] scale Q_V for vector-meson electroproduction in the non-asymptotic region, with

$$Q_V^2 = (Q^2+M_V^2)/4\,. \tag{65}$$

As explained in Sec. 4.2.4, the twist-decomposition parameter $\beta = M_V/Q$ is not really small in the kinematic region of the HERMES experiment. Therefore, HERMES results on amplitude ratios are expected to be not always in agreement with the pQCD predictions given by Eqs. (61-64). In the case of a disagreement, we use a parameterization that does not contradict general principles and describes the amplitude ratios with reasonable χ^2 per degree of freedom. Any NPE amplitude ratio has to obey Eq. (60). On very general principles, at finite Q the amplitudes T_{11}, T_{01}, and T_{1-1} are even functions in Q. In contrast, the amplitudes T_{00} and T_{10} are odd functions in Q due to the extra factor $1/Q$ in Eq. (12). Therefore, the ratios t_{11}, t_{01}, and t_{1-1} (t_{10}) are odd (even) functions in Q. The fit functions will be chosen in agreement with this property of amplitude ratios. Whenever the chosen fit function does not agree with a pQCD prediction, the resulting curve is shown not by a solid but a dash-dotted line.

7.2 Kinematic Dependence of T_{11}/T_{00}

The amplitudes T_{00} and T_{11} describe the diagonal helicity transitions $\gamma_L^* \to \rho_L^0$ and $\gamma_T^* \to \rho_T^0$ respectively, and are the largest amplitudes of ρ^0 meson production in the HERMES kinematic region. The Q^2 dependence of the extracted amplitude ratio t_{11} in four $-t'$ bins is presented in Fig. 4 for the proton (left) and the deuteron (right). The points correspond to the amplitude ratios extracted from the data in 16 bins and given in Tabs. 2 and 3. In order to test the predictions of Refs. [30,31], the Q^2 dependence of the ratio $\mathrm{Re}(t_{11})$ was fitted in every $-t'$ bin with the function

$$\mathrm{Re}(t_{11}) = \frac{a}{Q}. \tag{66}$$

For the four $-t'$ bins, the values of the parameter a are found to be consistent with each other within experimental accuracy. Therefore, data in all $-t'$ bins are fitted simultaneously to improve the statistical accuracy in determining the value of a. The results of the fit for proton and deuteron data are presented in Tab. 4 and shown in Fig. 4 for proton (left) and deuteron (right). The figure shows that the Q^2 dependence of $\mathrm{Re}(t_{11})$ is well described by the parameterization given by Eq. (66).

The dependences of the other amplitude ratios, which are described in the following, are examined in a similar manner as was done for $\mathrm{Re}(t_{11})$. In every case, it was checked that the respective four datasets containing 4 points each can be combined into one dataset containing 16 points. When proton and deuteron results are consistent, the data are combined and 32 points are used in the fit. All the fits to the Q^2 or t' dependences use 16 data points for the proton or deuteron separately and 32 data points for the combined data sets. Only for the sake of a more clear representation of the kinematic dependence of amplitude ratios in one variable Q^2 (or t'), we average the values of the amplitude ratios $\mathcal{T} = t_{\lambda_V\lambda_\gamma}$ or $|u_{11}|$ over four $-t'$ (or Q^2) bins at the same value of Q^2 (or t') using the standard relations for the mean value $\langle\mathcal{T}\rangle$ and squared total uncertainty $(\delta\mathcal{T})^2$:

$$\langle\mathcal{T}\rangle = \frac{\sum_j \mathcal{T}_j/(\sigma_j)^2}{\sum_m 1/(\sigma_m)^2}\,, \tag{67}$$

$$(\delta\mathcal{T})^2 = \frac{1}{\sum_m 1/(\sigma_m)^2}\,. \tag{68}$$

Here, σ_j denotes the total uncertainty of $\mathcal{T}_j$ in the j^{th} bin and $\delta\mathcal{T}$ is the total uncertainty of the averaged ratio $\mathcal{T}$. The same formula (68) is applied for the calculation of the

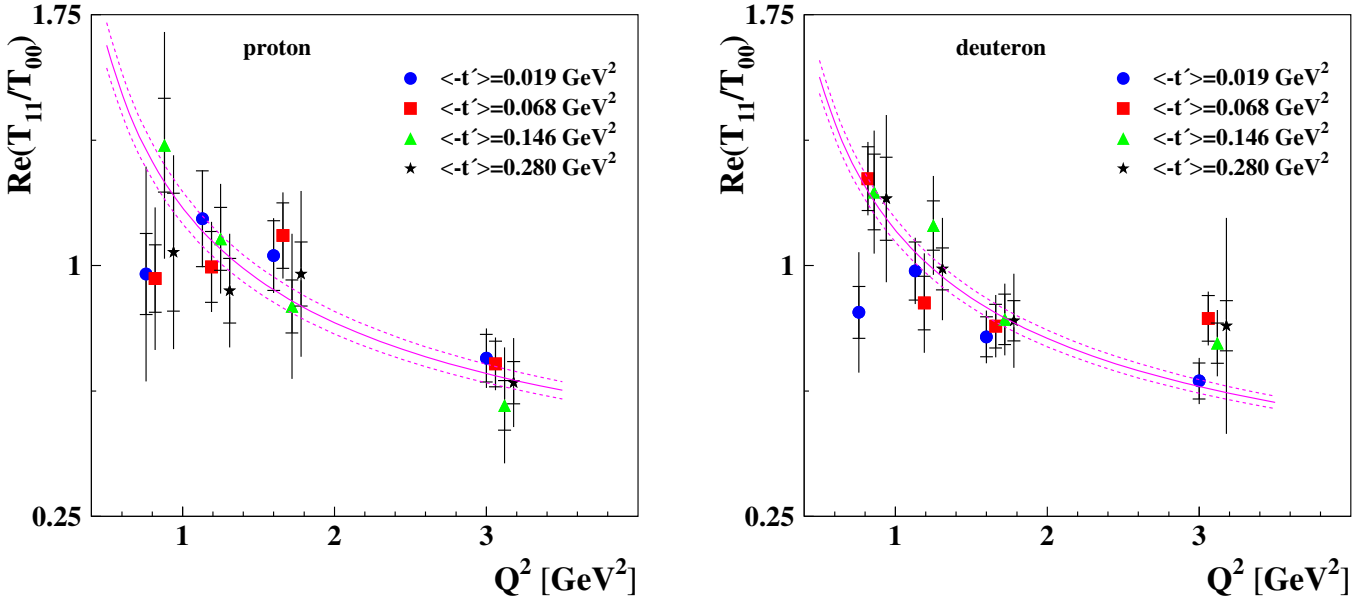

Fig. 4. The Q^2 dependence of $\mathrm{Re}(T_{11}/T_{00})$ for proton (left panel) and deuteron (right panel) data, showing the result for the 16 $(Q^2, -t')$ bins. Inner error bars show the statistical uncertainty and the total error bars represent statistical and systematic uncertainties added in quadrature. The parameterization of the curves is given by Eq. (66) and their parameters are given in Tab. 4. Central lines are calculated with the fitted values of parameters, while the dashed lines correspond to one standard deviation of the curve parameter. Except for the second $-t'$ bin, the data points are shifted for better visibility.

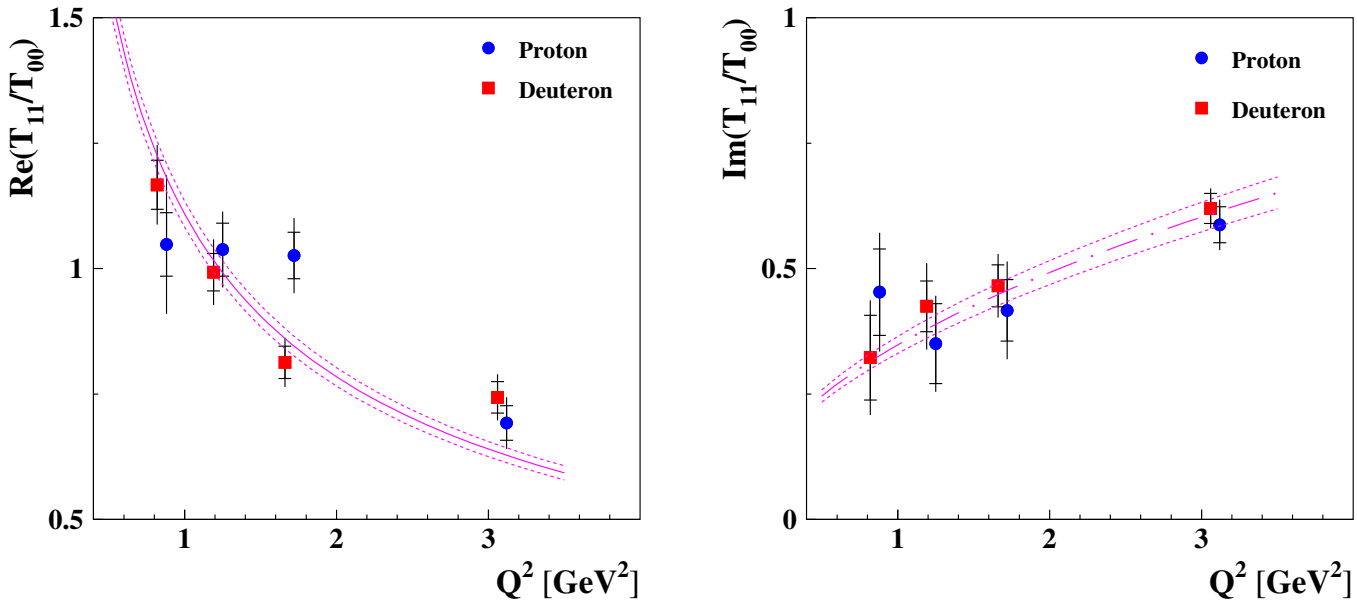

Fig. 5. The Q^2 dependence of $\mathrm{Re}(T_{11}/T_{00})$ (left panel) and $\mathrm{Im}(T_{11}/T_{00})$ (right panel) for proton and deuteron data. Points show the amplitude ratios from Tabs. 2 and 3 after averaging over four $-t'$ bins using Eqs. (67) and (68). The parameterization of the curves obtained from combined proton and deuteron data is given by Eqs. (66) and (69) while the parameters are given in Tab. 4. The meaning of the error bars and the explanation of the curves are the same as for Fig. 4. Here and hereafter proton data points are slightly displaced to the right for better visibility. As explained in the text, curves are shown as solid (dash-dotted) lines if the parameterization is based (not based) on pQCD predictions.

target	ratio	a, GeV	δa, GeV	χ^2/N_{df}
proton	$\mathrm{Re}(T_{11}/T_{00})$	1.173	± 0.048	0.63
deuteron	$\mathrm{Re}(T_{11}/T_{00})$	1.106	± 0.035	1.04
proton+deuteron	$\mathrm{Re}(T_{11}/T_{00})$	1.109	± 0.026	0.78
target	ratio	b, GeV^{-1}	δb, GeV^{-1}	χ^2/N_{df}
proton	$\mathrm{Im}(T_{11}/T_{00})$	0.340	± 0.025	0.54
deuteron	$\mathrm{Im}(T_{11}/T_{00})$	0.359	± 0.020	0.71
proton+deuteron	$\mathrm{Im}(T_{11}/T_{00})$	0.348	± 0.017	0.75

Table 4. The Q^2 dependence of $\mathrm{Re}(T_{11}/T_{00})$ and $\mathrm{Im}(T_{11}/T_{00})$ for proton, deuteron and combined data sets parameterized as given by Eqs. (66) and (69). The values of parameters with their total uncertainties are presented. The last column shows the value of χ^2 per degree of freedom.

statistical uncertainty $\delta\mathcal{T}_{stat}$ where σ_m is the statistical uncertainty of $\mathcal{T}_m$.

In the left panel of Fig. 5, the average values of the ratio $\mathrm{Re}(t_{11})$ in each of the Q^2 bins for both the proton and deuteron targets are shown. As the results for the two targets are found to be compatible, a fit to the combined proton and deuteron data is performed and the result extracted for a in Eq. (66) is also presented in Tab. 4. Reasonable values of χ^2 per degree of freedom, $\chi^2/N_{df} \approx 1$, are obtained. A comparison of the average values of ratio $\mathrm{Re}(t_{11})$ across $-t'$ bins and the curve calculated with Eq. (66) using the value of the parameter a obtained from the combined proton and deuteron data is shown in the left panel of Fig. 5. The Q^2 dependence of $\mathrm{Re}(t_{11})$ is found to be in a good agreement with the asymptotic behavior expected from pQCD.

As shown in the right panel of Fig. 5, the amplitude ratio $\mathrm{Im}(t_{11})$ rises with Q^2. This dependence of $\mathrm{Im}(t_{11})$ disagrees with the prediction [30,31] given by Eq. (61), whereas the dependence of the real part of the same ratio t_{11} agrees with predictions based on the same formula. A fit of the function in Eq. (66) to the experimental data does not provide reasonable values of χ^2 per degree of freedom: $\chi^2/N_{df} = 2.46$ for the proton data and $\chi^2/N_{df} = 4.25$ for the deuteron data. Instead, a fit function of the type

$$\mathrm{Im}(t_{11}) = bQ \tag{69}$$

gives reasonable results as can be seen from Tab. 4, where fit results for the proton, deuteron and combined datasets are presented. The right panel of Fig. 5 shows the curve calculated with the parameter b obtained for the combined proton and deuteron data compared with the $-t'$ bin averaged ratio $\mathrm{Im}(t_{11})$ for both proton and deuteron data. The disagreement with the prediction of Eq. (61) may be due to the fact that the Q^2 range of the HERMES experiment is not in the asymptotic region. This is in agreement with the conjecture of Ref. [31] that the hard scale for vector-meson electroproduction is Q_V given by Eq. (65) which is smaller than Q. Another possible explanation can be found in the discussion later in this paper of potential final-state interactions between the struck parton and the target remnant.

The phase difference δ_{11} between the helicity amplitudes T_{11} and T_{00} is given by the relation

$$\tan\delta_{11} = \mathrm{Im}(t_{11})/\mathrm{Re}(t_{11})\,. \tag{70}$$

It increases with Q^2 as shown in the left panel of Fig. 6. Also shown is a fit to the Q^2 dependence of δ_{11} calculated with the functional form $\tan\delta_{11} = bQ^2/a$ deduced from Eqs. (66) and (69). The result of the fit is $\delta_{11} = (31.5 \pm 1.4)$ degrees at $\langle Q^2\rangle = 1.95$ GeV^2, obtained with the parameters a and b given in Tab. 4 for the combined proton and deuteron data. It is consistent within one standard deviation with the published result [18] obtained with the SDME method using the same proton and deuteron data as in the present analysis. A large phase difference $\delta_{11} \approx 20$ degrees was measured by the H1 collaboration for exclusive ρ^0 and ϕ meson electroproduction at 2.5 GeV$^2 < Q^2 <$ 60 GeV^2 [20]. A large value of $\delta_{11} = (33.0 \pm 7.4)$ degrees was measured also in ϕ meson production at HERMES [51]. As two-gluon exchange dominates in ϕ meson production at HERMES kinematics, the measured large value of δ_{11} for ρ^0 cannot be attributed solely to the quark-antiquark exchange essential for ρ^0 meson production. This value of δ_{11} is in clear disagreement with a calculation [52] performed using a GPD-based approach in pQCD that predicts a very small value for δ_{11}. At present, there exists no model capable of explaining the value and Q^2 dependence of δ_{11}.

In existing pQCD calculations for exclusive vector-meson electroproduction, only two-gluon and/or quark-antiquark exchange have been taken into account. It can be argued [53] that even in inclusive deep-inelastic lepton-nucleon scattering, the final-state interaction of the struck quark alters the cross section due to multi-gluon exchanges with the target remnant. This is at variance with the traditional understanding obtained from inclusive DIS. It is shown [53] that a summation of multi-gluon-exchange amplitudes results in an eikonal-like correction. For vector-meson production, if rescattering on the nucleon occured also for the quark-antiquark pair that transforms to the final vector meson, the eikonal-like correction might be responsible for the measured large phases observed in the present work.

Figure 7 shows the t' dependence of the real and imaginary parts of the ratio t_{11}. Since $\mathrm{Re}(t_{11})$ and $\mathrm{Im}(t_{11})$ depend on Q^2 according to Eqs. (66) and (69), they are

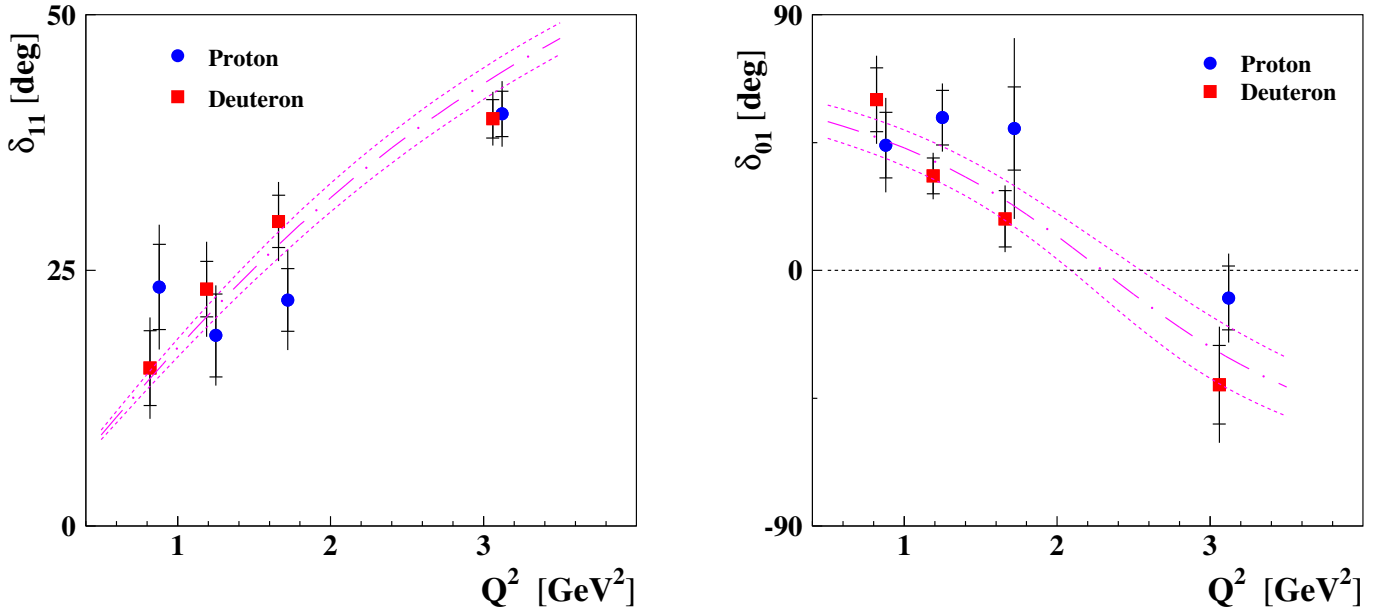

Fig. 6. The Q^2 dependence of the phase difference δ_{11} (left panel) and δ_{01} (right panel, see Sec. 7.4) between the amplitudes T_{11} and T_{01}, respectively, and T_{00} obtained for proton and deuteron data. Points show the phase differences δ_{11} and δ_{01} calculated from ratios of amplitudes given in Tabs. 2 and 3 after averaging over $-t'$ bins. Inner error bars show the statistical uncertainty and the outer ones show the statistical and systematic uncertainties added in quadrature. The fitted parameterization is given by Eqs. (70) and (78) respectively for δ_{11} and δ_{01}. The parameters of the curves are given in Tabs. 4 and 6 for combined proton and deuteron data. The central lines are calculated with the fitted values of the parameters, while the dashed lines correspond to one standard deviation in the uncertainty of the curve parameter.

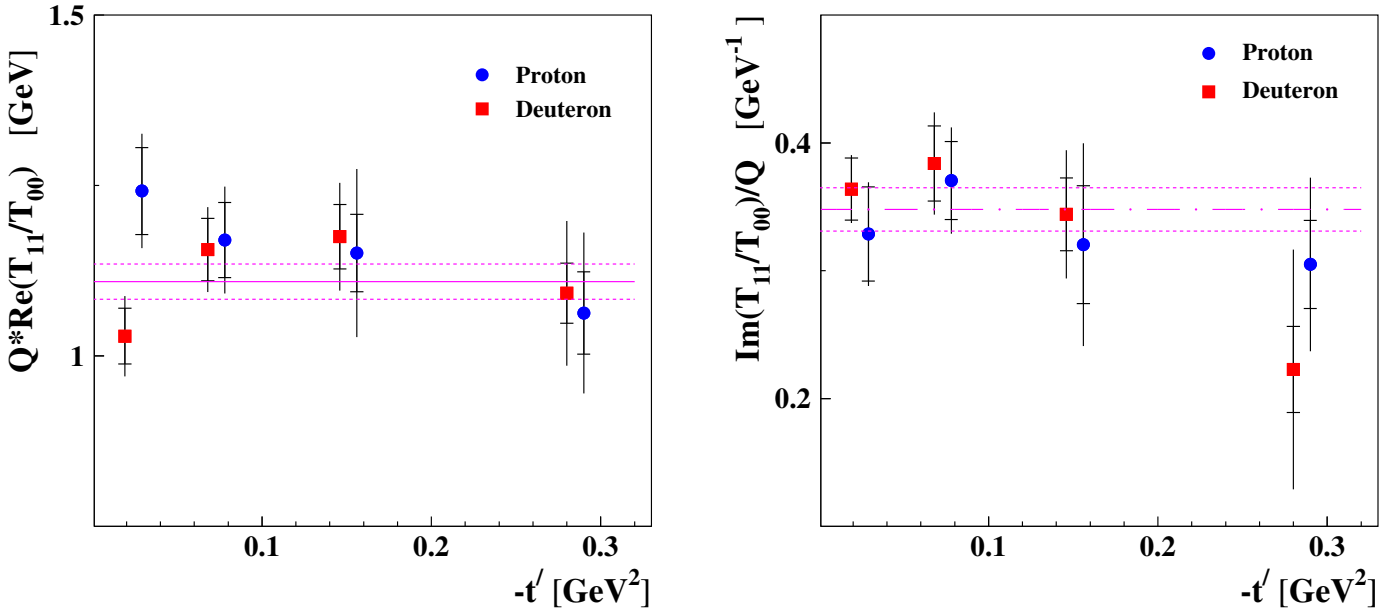

Fig. 7. The t' dependence of $Q \cdot \mathrm{Re}(T_{11}/T_{00})$ (left panel) and $\mathrm{Im}(T_{11}/T_{00})/Q$ (right panel) for proton and deuteron data. Points show the amplitude ratios from Tabs. 2 and 3 after averaging over four Q^2 bins using Eqs. (67) and (68). The straight lines in the left and right panel show the value of a and b, respectively, from Eqs. (66) and (69) while the parameters a and b are given in Tab. 4. The meaning of the error bars and the explanation of the curves are the same as for Fig. 4.

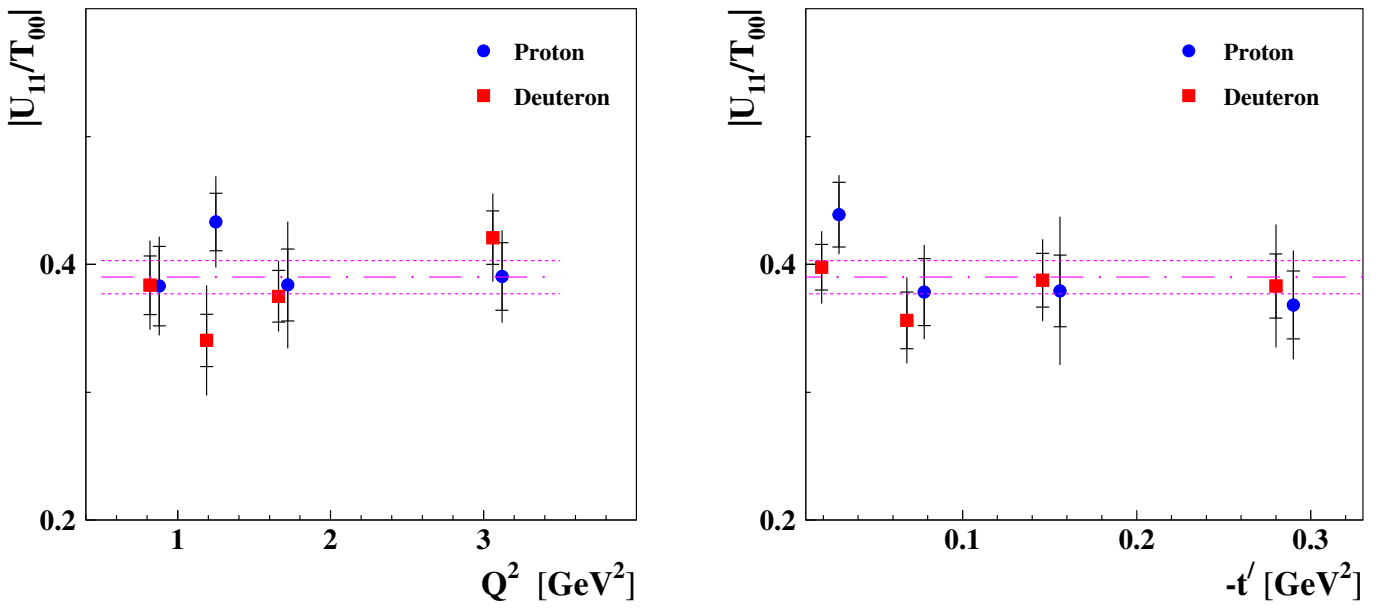

Fig. 8. The dependences of $|U_{11}/T_{00}|$ on Q^2 and t' for proton and deuteron data. The points show the amplitude ratios given in Tabs. 2 and 3 after averaging over $-t'$ (Q^2) bins in the left (right) panel. The inner error bars show the statistical uncertainty and the outer ones show the statistical and systematic uncertainties added in quadrature. The results fitting the combined data set with a constant (central line), $|U_{11}/T_{00}| = g$, are given in Tab. 5. The dashed lines correspond to one standard deviation in the total uncertainty.

target	ratio	g	δg	χ^2/N_{df}
proton	$\lvert U_{11}/T_{00}\rvert$	0.400	$\pm$0.020	0.60
deuteron	$\lvert U_{11}/T_{00}\rvert$	0.383	$\pm$0.017	0.40
proton+deuteron	$\lvert U_{11}/T_{00}\rvert$	0.390	$\pm$0.013	0.49

Table 5. Results of fitting the ratio $|U_{11}/T_{00}|$ to a constant for proton, deuteron and combined data sets. The values of parameters with their total uncertainties are presented. The last column shows the value of χ^2 per degree of freedom.

shown in Fig. 7 multiplied or divided by Q, respectively. No noticeable t' dependence is observed for $\mathrm{Re}(t_{11})$ and $\mathrm{Im}(t_{11})$. Since the differential cross section of the process in Eq. (1) for high energies and small $|t'|$ is usually described by an exponential factor $\exp\{\beta t'\}$, the helicity amplitudes should have exponential factors $T_{00} \propto \exp\{\beta_L t'/2\}$ and $T_{11} \propto \exp\{\beta_T t'/2\}$. The absence of a t' dependence of the ratio T_{11}/T_{00} means that the slope parameters β_L and β_T for the amplitudes T_{00} and T_{11} are close to each other. For very small $|t'|$, it is reasonable to use the linear approximation

$$\mathrm{Re}(T_{11}/T_{00}) = \frac{a}{Q}\exp\{-\frac{1}{2}\Delta\beta_1 t'\} \approx \frac{a}{Q}(1+\frac{1}{2}\Delta\beta_1|t'|), \quad (71)$$

$$\mathrm{Im}(T_{11}/T_{00}) = bQ\exp\{-\frac{1}{2}\Delta\beta_2 t'\} \approx bQ(1+\frac{1}{2}\Delta\beta_2|t'|). \quad (72)$$

The proton results are $\Delta\beta_1 = (-1.02 \pm 0.85)$ GeV^{-2} and $\Delta\beta_2 = (-0.91 \pm 2.00)$ GeV^{-2}, while the fit for the deuteron data gives $\Delta\beta_1 = (0.58 \pm 0.80)$ GeV^{-2} and $\Delta\beta_2 = (-1.96 \pm 1.58)$ GeV^{-2}. The results of the fits show that all four numbers are consistent with one another. We now assume that, within experimental accuracy, the slope parameters for the real and imaginary parts of the ratio coincide across both target types. In this case we have $\Delta\beta_1 \approx \Delta\beta_2 \approx \beta_L - \beta_T$. Combining these four numbers making use of Eqs. (67) and (68) we get an estimate for $\beta_L - \beta_T = (-0.4 \pm 0.5)$ GeV^{-2}. This result on $\beta_L - \beta_T$ is in agreement with the prediction published in Ref. [54], which ranges from -0.7 GeV^{-2} at $Q^2 = 0.8$ GeV^2 to -0.4 GeV^{-2} at $Q^2 = 5$ GeV^2.

7.3 Kinematic Dependence of $|U_{11}/T_{00}|$

The unnatural-parity-exchange amplitude, U_{11}, describes the transition from a transversely polarized photon to a transversely polarized ρ^0 meson ($\gamma_T^* \to \rho_T^0$). At large W

target	ratio	c, GeV^{-1}	δc, GeV^{-1}				χ^2/N_{df}
proton	Re(T_{01}/T_{00})	0.405	$\pm$0.046				0.56
deuteron	Re(T_{01}/T_{00})	0.378	$\pm$0.033				0.69
proton+deuteron	Re(T_{01}/T_{00})	0.394	$\pm$0.024				0.63
target	ratio	f	δf				χ^2/N_{df}
proton	Im(T_{01}/T_{00})	0.317	$\pm$0.115				0.97
deuteron	Im(T_{01}/T_{00})	0.161	$\pm$0.090				1.20
proton+deuteron	Im(T_{01}/T_{00})	0.221	$\pm$0.069				1.10
target	ratio	f_1 GeV^{-1}	δf_1 GeV^{-1}	f_2 GeV^{-3}	δf_2 GeV^{-3}	ρ_c	χ^2/N_{df}
proton+deuteron	Im(T_{01}/T_{00})	0.653	$\pm$0.132	-0.285	$\pm$0.065	-0.903	0.66

Table 6. The kinematic dependence of Re(T_{01}/T_{00}) and Im(T_{01}/T_{00}) for the proton, deuteron and combined data sets parameterized as given by Eqs. (74 – 76). The values of parameters with their total uncertainties are presented. The last column shows the value of χ^2 per degree of freedom and ρ_c is the correlation parameter.

and Q^2, this transition should be suppressed by a factor of M_V/Q compared to the dominant amplitude T_{00} as explained in Sec. 4.2.2. The UPE contributions to the amplitude may be sizable at intermediate energies [35,36] typical for HERMES.

The ratio $|u_{11}|$ versus Q^2 and t' is presented in Fig. 8. The value of $|U_{11}|$ is found to be smaller than $|T_{00}|$ by a factor of approximately 2.5. No kinematic dependences of the ratio $|u_{11}|$ are seen and therefore it is fitted to a constant

$$|u_{11}| = g. \tag{73}$$

The results of the fit to proton and deuteron combined data are given in Tab. 5, and the constant g is shown in Fig. 8 by straight lines. Fits with the same function a/Q as for Re(t_{11}) (see Eq. (66)), corresponding to the behavior expected in pQCD, give values for χ^2 per degree of freedom 2.03, 2.67, and 2.25 for the proton, deuteron, and combined data, respectively. This disagreement may reflect the fact that the HERMES Q^2 region is far from the asymptotic one.

From a study of soft hadron scattering, it is known [35, 36,55] that the most important contribution to UPE amplitudes at intermediate energies comes from pion exchange. The amplitude of one-pion-exchange in the t-channel contains the propagator $1/(t - m_\pi^2)$, which become large for small values of $-t$ that approach the pole at the unphysical value of $-t = -m_\pi^2 \approx -0.018$ GeV^2. The mean value of $-t'$ for the first $-t'$ bin is 0.019 GeV^2, and hence might appear to be small enough to approach the vicinity of the pole. However, as shown in the right panel of Fig. 8, no evidence for a pion-pole-like dependence can be seen in the data within the statistical precision of the measurement. Such a dependence could be weakened by various effects:
i) even in the first bin in $-t'$, the value of $\langle -t \rangle$ equal to 0.06 GeV^2 is substantial, and hence not close enough to the pion pole at unphysical positive t,
ii) the amplitude T_{00} has a strong exponential dependence $\propto \exp\{\beta_L t'/2\}$ with $\beta_L \approx 7$ GeV^{-2} [18,47] and decreases with $|t'|$, hence the ratio U_{11}/T_{00} is flatter than U_{11} itself,
iii) in addition to one-pion exchange, other exchange processes can contribute to the amplitude U_{11}.

Using the amplitude method, the signal of unnatural-parity exchange has a significance of more than 20 standard deviations in the total experimental uncertainty separately for each of the proton and deuteron data sets (see Tab. 5 and Fig. 8). In contrast, the existence of UPE was established [18] with a significance of 3 standard deviations for the combined proton and deuteron data in the analysis using the SDME method.

7.4 Kinematic dependence of T_{01}/T_{00}

The amplitude $T_{01} \equiv T_{0\frac{1}{2}1\frac{1}{2}}$ describing the transition $\gamma_T^* \to \rho_L^0$ is expected to be the largest SCHC-violating amplitude. In accordance with the asymptotic formula (62), the parameterization

$$\mathrm{Im}(t_{01}) = f\frac{\sqrt{-t'}}{Q} \tag{74}$$

is used. A fit to both proton and deuteron data using this parameterization gives acceptable χ^2 values, as seen in Tab. 6. Proton and deuteron results are compatible within one standard deviation in the total uncertainty, although neither measurement is particularly precise as shown in Tab. 6 and the right panel of Fig. 9 in which the data are multiplied by Q in order to demonstrate the $\sqrt{-t'}$ dependence. The fit of the combined proton and deuteron data set yields a value of the parameter f that is three standard deviations from zero with $\chi^2/N_{df} \approx 0.66$ (see Tab. 6). We note that these results do not necessarily confirm the validity of Eq. (62) although the data do not contradict the pQCD prediction.

The Q^2 dependence of the amplitude ratio Im(t_{01}) for the proton and deuteron data is shown in the right panel of Fig. 10. As shown in the figure, the point for the deuteron in the largest Q^2 bin is slightly negative which favours a fit using the equation

$$\mathrm{Im}(t_{01}) = \sqrt{-t'}(f_1 + f_2 Q^2) \tag{75}$$

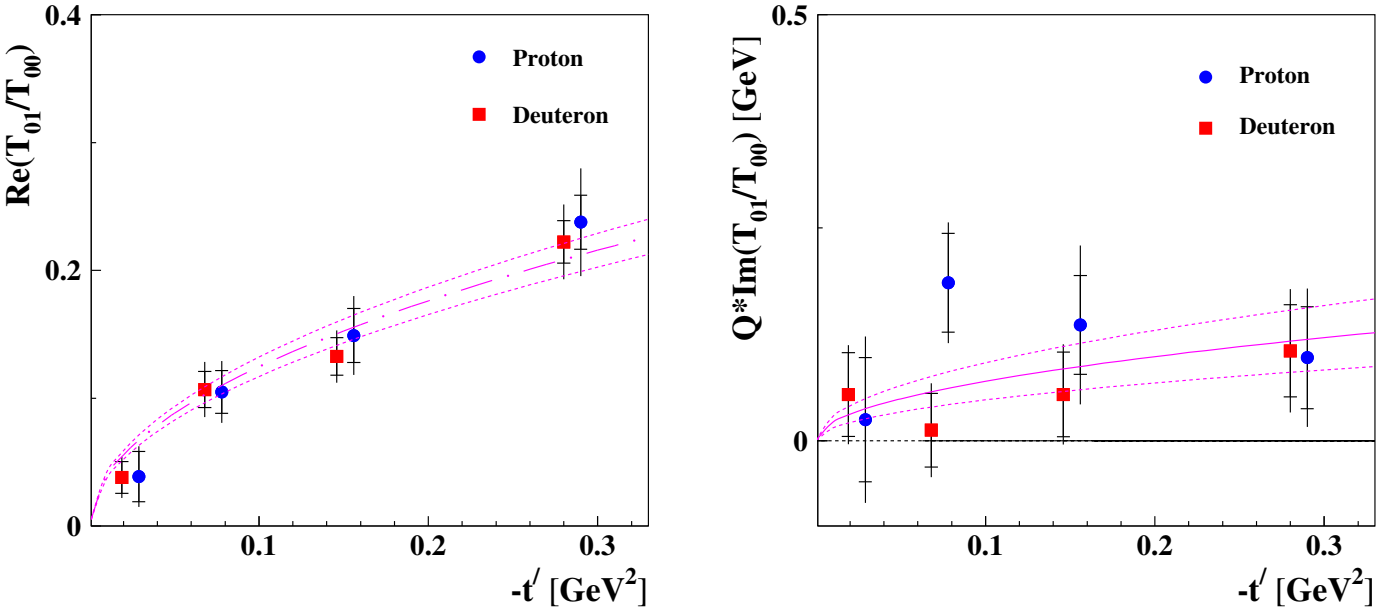

Fig. 9. The t' dependence of $\mathrm{Re}(T_{01}/T_{00})$ (left panel) and $Q \cdot \mathrm{Im}(T_{01}/T_{00})$ (right panel) for proton and deuteron data. Points show amplitude ratios from Tabs. 2 and 3 after averaging over Q^2 bins. Inner error bars show the statistical uncertainty and the outer bars show statistical and systematic uncertainties added in quadrature. The parameterization is given by Eqs. (74) and (76). The parameters of the curves are given in Tab. 6 for combined proton and deuteron data. Central lines are calculated with fitted values of parameters, while the dashed lines correspond to one standard deviation of the curve parameter.

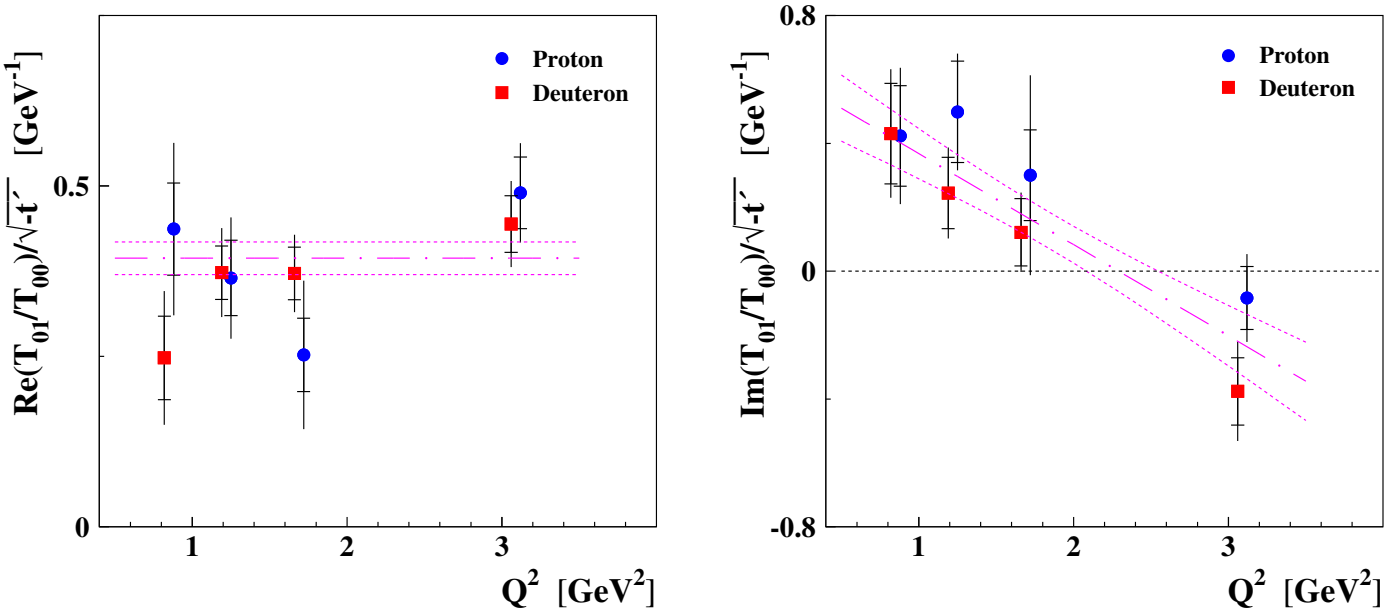

Fig. 10. The Q^2 dependence of $\mathrm{Re}(T_{01}/T_{00})/\sqrt{-t'}$ (left panel) and $\mathrm{Im}(T_{01}/T_{00})/\sqrt{-t'}$ (right panel) for proton and deuteron data. Points show amplitude ratios from Tabs. 2 and 3 after averaging over $-t'$ bins. Inner error bars show the statistical uncertainty and the outer bars show statistical and systematic uncertainties added in quadrature. The parameterization is given by Eqs. (75) and (76). The parameters of the curves are given in Tab. 6 for combined proton and deuteron data. Central lines are calculated with fitted values of parameters, while the dashed lines correspond to one standard deviation of the curve parameter.

over that using parameterization (74). The result of the fit with function (75) is shown in the right panel of Fig. 10. The parameters f_1 and f_2 are strongly correlated. The correlation parameter ρ_c is presented in Tab. 6 and is taken into account in the calculation of the uncertainty of $\mathrm{Im}(t_{01})$ using Eq. (75).

The Q^2 dependence of the ratio $\mathrm{Re}(t_{01})/\sqrt{-t'}$ is presented in the left panel of Fig. 10. The quantity $\mathrm{Re}(t_{01})/\sqrt{-t'}$ does not decrease with Q^2 and can be well described by a constant which is also shown in the figure. Using for $\mathrm{Re}(t_{01})$ the functional form of Eq. (74) yields χ^2/N_{df} values of 1.08, 1.55, and 1.31 for separate fits to the proton, deuteron and combined data sets. Using instead the simpler parameterization

$$\mathrm{Re}(t_{01}) = c\sqrt{-t'} \tag{76}$$

decreases the value of χ^2 by a factor of approximately two, indicating a better description of the data. The results of this fit are shown in Tab. 6 and the left panels of Figs. 9 and 10. The small values of χ^2/N_{df} as shown in Tab. 6 indicate that our systematic uncertainty might be overestimated.

The phase difference δ_{01} between the amplitudes T_{01} and T_{00} can be calculated using the formula

$$\tan\delta_{01} = \mathrm{Im}(t_{10})/\mathrm{Re}(t_{10}). \tag{77}$$

The results for the Q^2 dependence of δ_{01} after averaging over $-t'$ bins are shown in the right panel of Fig. 6. The phase difference δ_{01} is non-zero and decreases with Q^2. It is slightly negative for the deuteron data at the largest value of Q^2. Using instead the results from the fits to formulas (75, 76) given in Tab. 6, the phase difference is obtained as

$$\tan\delta_{01} = (f_1 + f_2 Q^2)/c\,, \tag{78}$$

which is shown as a curve in the right panel of Fig. 6. As can be seen, the fit function (78) is able to describes the Q^2 dependence of the phase difference δ_{01}.

7.5 Small Amplitude Ratios T_{10}/T_{00} and T_{1-1}/T_{00}

According to the hierarchy given in Eq. (31), T_{10} and T_{1-1} are the smallest amplitudes that give linear contributions to the numerators of SDMEs in the case of an unpolarized target. The ratio t_{10} is expected to be proportional to $\sqrt{-t'}$ in accordance with Eq. (60), while t_{1-1} is expected to be proportional to t'. These ratios are supposed to depend on Q^2 in the asymptotic region according to Eqs. (63) and (64). Figure 11 shows $\mathrm{Re}(t_{10})/\sqrt{-t'}$ and $\mathrm{Im}(t_{10})/\sqrt{-t'}$ versus Q^2 for both proton and deuteron data. As shown in Fig. 11, the values of $\mathrm{Re}(t_{10})/\sqrt{-t'}$ and $\mathrm{Im}(t_{10})/\sqrt{-t'}$ on the proton are compatible with zero. The results of the fit of $\mathrm{Re}(t_{10})$ with the function

$$\mathrm{Re}(t_{10}) = r\sqrt{-t'} \tag{79}$$

and $\mathrm{Im}(t_{10})$ with the same function are presented in Tab. 7. The ratio $\mathrm{Re}(t_{10})/\sqrt{-t'}$ for the deuteron is slightly positive (except the first point at the smallest value of Q^2) and increases with Q^2. The fit of the deuteron data with the function

$$\mathrm{Re}(t_{10}) = sQ^2\sqrt{-t'} \tag{80}$$

provides the positive result which is presented in Tab. 7. As shown in Fig. 11, the quantity $\mathrm{Im}(t_{10})/\sqrt{-t'}$ is negative for the three points at the largest values of Q^2. The fit of $\mathrm{Im}(t_{10})/\sqrt{-t'}$ using the same function (80) gives the negative result presented in Tab. 7. This behavior contradicts the pQCD prediction given by Eq. (63), and indicates that in the case of the amplitude T_{10} the HERMES kinematic range may be far from the large-Q asymptotic region.

We recall that the amplitudes T_{00} and T_{10} vanish in the small Q-limit ($Q^2 \to 0$) because the real photon has no longitudinal polarization. If the behavior at fixed t' and small Q^2 were described by

$$T_{00} \propto Q\,, \tag{81}$$
$$T_{10} \propto Q^3, \tag{82}$$

the behavior of the ratio $t_{10} \equiv T_{10}/T_{00}$ would be just as assumed by Eq. (80) and presented in Fig. 11.

The ratios $\mathrm{Re}(t_{1-1})/(-t')$ and $\mathrm{Im}(t_{1-1})/(-t')$ are presented versus Q^2 in Fig. 12. Both ratios appear to be compatible with zero within 2.5 σ of the total uncertainty both for the proton and deuteron target and only the combined data provides a non-zero signal for $\mathrm{Im}(t_{1-1})$. The fit of $\mathrm{Re}(t_{1-1})$ with the function

$$\mathrm{Re}(t_{1-1}) = (-t')\frac{h}{Q} \tag{83}$$

corresponds to the second term in Eq. (64). The result, presented in Tab. 8 for the combined proton and deuteron data, shows a signal of 2σ significance with respect to the total uncertainty. The result of the fit of $\mathrm{Im}(t_{1-1})$ with the same function (83) is also presented in Tab. 8. The parameter h deviates from zero by more than three standard deviations of the total uncertainty. A fit of the combined proton and deuteron data with both terms in Eq. (64) provides values of C_1 and C_2 that are consistent with zero within 1.5 σ of the total uncertainty for both $\mathrm{Re}(t_{1-1})$ and $\mathrm{Im}(t_{1-1})$. This means that the statistical precision of the HERMES data does not allow a reliable verification of Eq. (64) or an extraction of the gluon transversity GPD.

7.6 Comparison of HERMES and H1 Results

Here we compare the results of the present work with the analysis of the ρ^0-meson production data on the proton by the H1 collaboration [20], obtained for the CM energy range 36 GeV $\leq W \leq$ 180 GeV, photon virtuality 2.5 GeV$^2 \leq Q^2 \leq$ 60 GeV^2, and $-t' \leq 3$ GeV^2. For the comparison of the t' dependence, the results at the mean value of Q^2 equal to 3.3 GeV^2 are chosen which are the

target	ratio	r, GeV^{-1}	δr, GeV^{-1}	χ^2/N_{df}
proton	Re(T_{10}/T_{00})	-0.012	±0.030	1.07
proton	Im(T_{10}/T_{00})	0.019	±0.061	0.58
target	ratio	s, GeV^{-3}	δs, GeV^{-3}	χ^2/N_{df}
deuteron	Re(T_{10}/T_{00})	0.045	±0.015	0.32
deuteron	Im(T_{10}/T_{00})	-0.109	±0.021	1.02

Table 7. The kinematic dependences of Re(T_{10}/T_{00}) and Im(T_{10}/T_{00}) for proton and deuteron parameterized as given by Eqs. (79) and (80). The values of parameters with their total uncertainties are presented. The last column shows the value of χ^2 per degree of freedom.

target	ratio	h, GeV^{-1}	δh, GeV^{-1}	χ^2/N_{df}
proton+deuteron	Re(T_{1-1}/T_{00})	-0.156	±0.059	0.79
proton+deuteron	Im(T_{1-1}/T_{00})	-0.418	±0.126	0.54

Table 8. The kinematic dependence of Re(T_{1-1}/T_{00}) and Im(T_{1-1}/T_{00}) for combined proton and deuteron data parameterized as given by Eq. (83). The values of parameters with their total uncertainties are presented. The last column shows the value of χ^2 per degree of freedom.

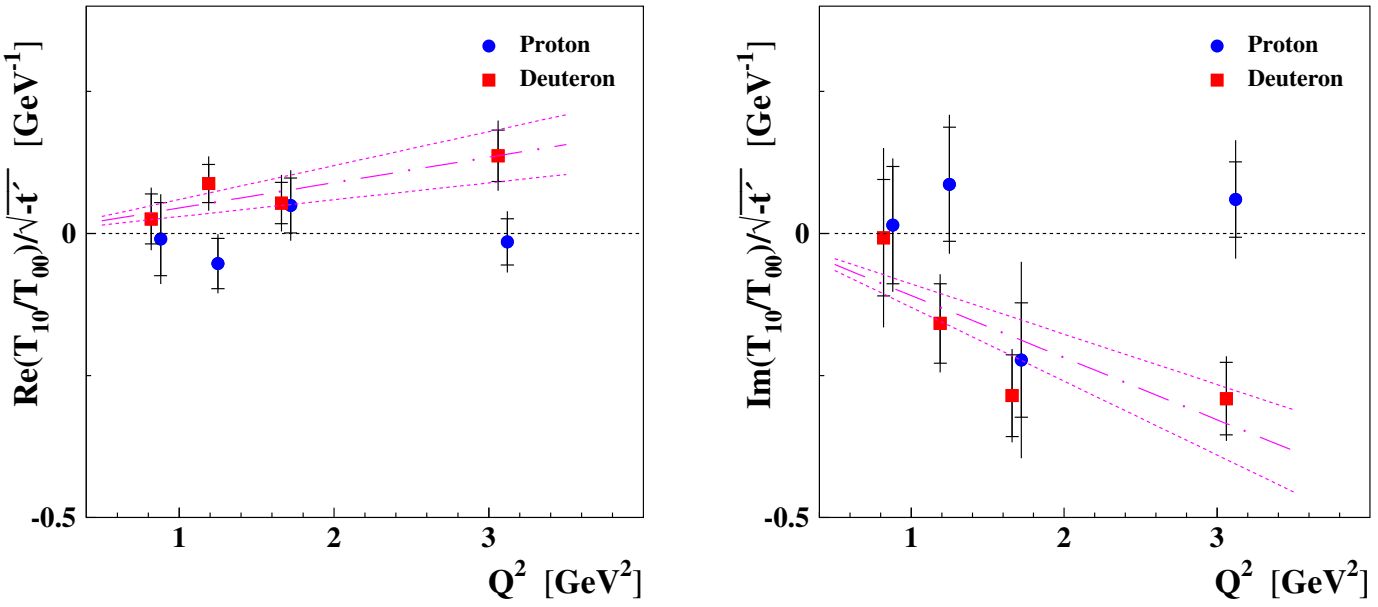

Fig. 11. The Q^2 dependence of Re(T_{10}/T_{00})/$\sqrt{-t'}$ (left panel) and Im(T_{10}/T_{00})/$\sqrt{-t'}$ (right panel) for proton and deuteron data. Points show amplitude ratios from Tabs. 2 and 3 after averaging over $-t'$ bins. Inner error bars show the statistical uncertainty and the outer ones indicate statistical and systematic uncertainties added in quadrature. The parameterization of the curves describing the deuteron data both on Re(T_{10}/T_{00}) and Im(T_{10}/T_{00}) is given by Eq. (80) and their parameters are given in Tab. 7. Central lines are calculated with the fitted values of parameters, while the dashed lines correspond to one standard deviation of the curve parameter.

closest ones to the Q^2 region of the HERMES data. In the H1 data analysis presented in Ref. [20], the imaginary parts of the amplitude ratios were not extracted. The additional hypothesis was used in Ref. [20] that for any ratio of the amplitudes, the approximate relation $|t_{\lambda_V\lambda_\gamma}|^2 = [\mathrm{Re}(t_{\lambda_V\lambda_\gamma})]^2$ is valid within the experimental accuracy. The comparison of the HERMES and H1 results is presented in Fig. 13. As seen from the figure the HERMES and H1 results agree within their total uncertainties. No strong dependence on W is observed for the amplitude ratios Re(t_{11}) and Re(t_{01}). Considering the differences in Q^2 between HERMES ($\langle Q^2\rangle$ = 2.0 GeV^2) and H1 ($\langle Q^2\rangle$ = 3.3 GeV^2), no Q^2 dependence can be seen for Re(t_{01}) at small $|t'|$ even for $Q^2 \leq 3.3$ GeV^2 (see also the discussion in Sec. 7.4). The ratios Re(t_{10}) and Re(t_{1-1}) obtained by H1 [20] are compatible with zero at $Q^2 = 3.1$

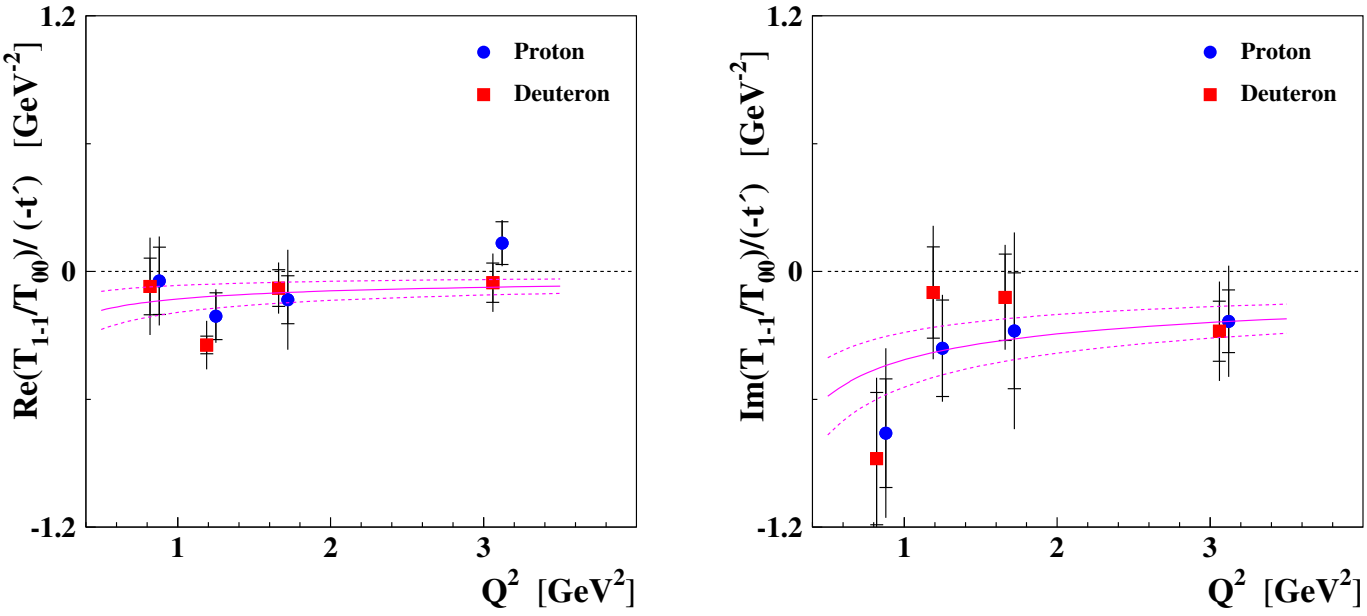

Fig. 12. The Q^2 dependence of $\mathrm{Re}(T_{1-1}/T_{00})/(-t')$ (left panel) and $\mathrm{Im}(T_{1-1}/T_{00})/(-t')$ (right panel) for proton and deuteron data. Points show amplitude ratios from Tabs. 2 and 3 after averaging over $-t'$ bins. Inner error bars show the statistical uncertainty and the outer ones indicate statistical and systematic uncertainties added in quadrature. The parameterization of the curves describing the combined proton and deuteron data both on $\mathrm{Re}(T_{1-1}/T_{00})$ and $\mathrm{Im}(T_{1-1}/T_{00})$ is given by Eq. (83) and their parameters are given in Tab. 8. Central lines are calculated with the fitted values of parameters, while the dashed lines correspond to one standard deviation of the curve parameter.

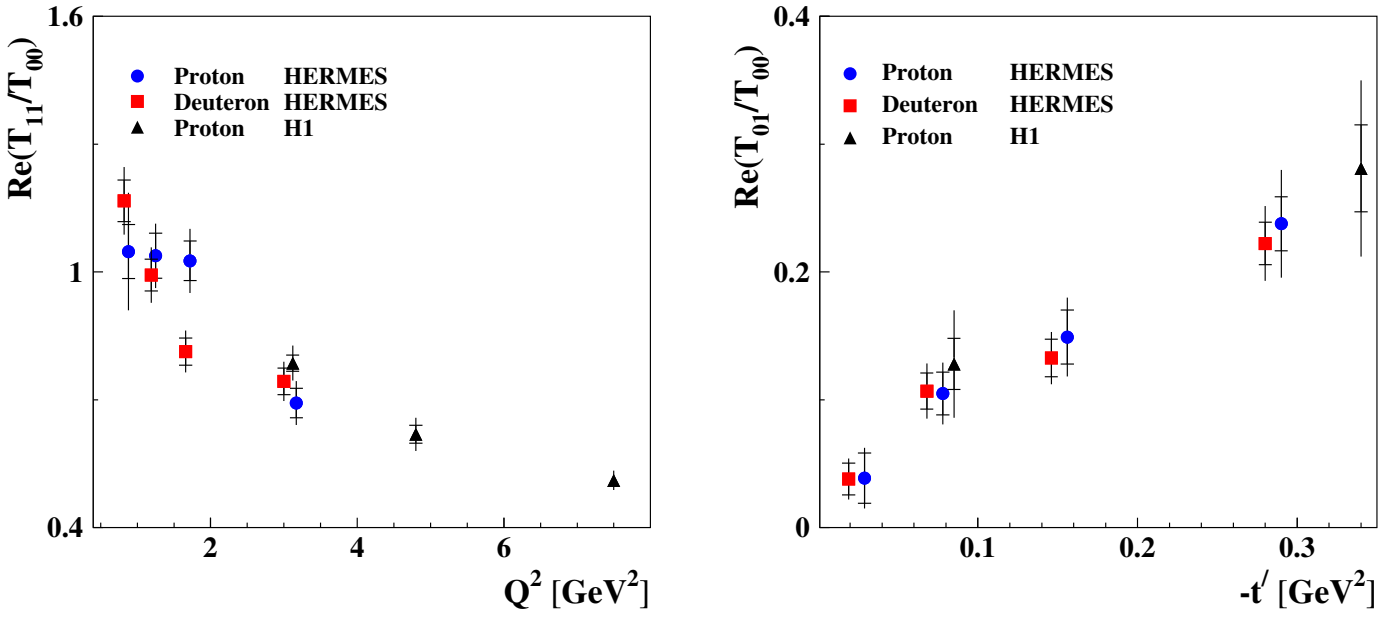

Fig. 13. The kinematic dependences of $\mathrm{Re}(T_{11}/T_{00})$ and $\mathrm{Re}(T_{01}/T_{00})$ for proton and deuteron data. Points of HERMES are the same as in Figs. 5 and 9. The H1 results are from Ref. [20]. Inner error bars show the statistical uncertainty and the outer ones indicate statistical and systematic uncertainties added in quadrature.

GeV^2 within the experimental accuracy. This is consistent with the HERMES results for the proton shown in Figs. 11 and 12.

8 Conclusions

Exclusive ρ^0-meson electroproduction is studied in the HERMES experiment, using a 27.6 GeV longitudinally polarized electron/positron beam and unpolarized hydrogen and deuterium targets in the kinematic region $0.5\ \mathrm{GeV}^2 < Q^2 < 7.0\ \mathrm{GeV}^2$, $3.0\ \mathrm{GeV} < W < 6.3\ \mathrm{GeV}$, and $-t' < 0.4\ \mathrm{GeV}^2$. These data are used to determine the real and imaginary parts of the ratios T_{11}/T_{00}, T_{01}/T_{00}, T_{10}/T_{00}, T_{1-1}/T_{00}, and $|U_{11}/T_{00}|$ for 16 bins in Q^2 and $-t'$. Systematic uncertainties due to the background contribution, uncertainties in the Monte Carlo input parameters, and the uncertainty of the applied amplitude method are given. Except for T_{10}/T_{00}, the amplitude ratios for the proton are compatible with those for the deuteron. The extracted amplitude ratios T_{11}/T_{00}, $|U_{11}/T_{00}|$ and T_{01}/T_{00} are found to be sizable. The ratios T_{10}/T_{00} and T_{1-1}/T_{00} for the proton are found to be compatible with zero within experimental uncertainties. The ratio T_{1-1}/T_{00} for the deuteron is also zero within experimental accuracy, while $\mathrm{Re}(T_{10}/T_{00})$ is slightly positive and $\mathrm{Im}(T_{10}/T_{00})$ is slightly negative, except for the bin with the smallest Q^2 values.

The SDMEs calculated in terms of these helicity amplitude ratios generally agree with the results published in Ref. [18]. The amplitude method was shown to provide more accurate polarized SDMEs than the previous analysis using the SDME method.

The statistical precision available in this analysis permits the parameterization of the kinematic dependences of amplitude ratios and the extraction of the phase difference between various helicity amplitudes. The real part of T_{11}/T_{00} is found to follow the asymptotic $1/Q$ behavior predicted by pQCD [30,31]. The imaginary part of T_{11}/T_{00} grows with Q^2, in contradiction to the large-Q^2 asymptotic behavior expected from pQCD. The phase difference δ_{11} between the amplitudes T_{11} and T_{00} grows with Q^2 and has a mean value of about 30 degrees in the HERMES kinematic region. This is in agreement with the published result of the SDME method [18] and in contradiction to calculations [11,12,13,30,31] based on pQCD. For the first time, the Q^2 dependence of δ_{11} observed in Ref. [18] is shown to be related to the increase with Q^2 of the imaginary part of the ratio of the helicity amplitudes T_{11}/T_{00}.

The behavior of $\mathrm{Im}(T_{01}/T_{00})$ is found to be in agreement with the asymptotic pQCD behavior $\sqrt{-t'}/Q$, while the extracted value of $\mathrm{Re}(T_{01}/T_{00})$ is likely to be in disagreement with the pQCD prediction. The data indicate non-zero values of the phase difference δ_{01} between the amplitudes T_{01} and T_{00} and the decrease of δ_{01} with Q^2.

The ratio $|U_{11}/T_{00}|$ is found to be constant in the HERMES kinematic region, in disagreement with the asymptotic pQCD behavior at large Q^2. No pion-pole-like behavior is observed at small $|t'|$. The UPE signal is seen with a very high significance for both proton and deuteron data, confirming the existence of unnatural-parity exchange contributions with a higher precision than that obtained with the SDME method [18].

The Q^2 dependence of the amplitude ratio $\mathrm{Re}(T_{11}/T_{00})$ and t' dependence of the amplitude ratio $\mathrm{Re}(T_{01}/T_{00})$ are also compared to those extracted by the H1 collaboration at the center-of-mass energy range $36\ \mathrm{GeV} \leq W \leq 180\ \mathrm{GeV}$, photon virtuality $2.5\ \mathrm{GeV}^2 \leq Q^2 \leq 60\ \mathrm{GeV}^2$, and $-t' \leq 3\ \mathrm{GeV}^2$. No strong dependence of the amplitude ratios $\mathrm{Re}(T_{11}/T_{00})$ and $\mathrm{Re}(T_{01}/T_{00})$ on W, and no Q^2 dependence of $\mathrm{Re}(t_{01})$ at small $|t'|$ are observed. The HERMES and H1 results agree within their total uncertainties.

Acknowledgments

We would like to thank M. Diehl, S.V. Goloskokov, P. Hoyer, and P. Kroll for many useful discussions.

We gratefully acknowledge the DESYmanagement for its support and the staff at DESY and the collaborating institutions for their significant effort. This work was supported by the Ministry of Economy and the Ministry of Education and Science of Armenia; the FWO-Flanders and IWT, Belgium; the Natural Sciences and Engineering Research Council of Canada; the National Natural Science Foundation of China; the Alexander von Humboldt Stiftung, the German Bundesministerium für Bildung und Forschung (BMBF), and the Deutsche Forschungsgemeinschaft (DFG); the Italian Istituto Nazionale di Fisica Nucleare (INFN); the MEXT, JSPS, and G-COE of Japan; the Dutch Foundation for Fundamenteel Onderzoek der Materie (FOM); the Russian Academy of Science and the Russian Federal Agency for Science and Innovations; the U.K. Engineering and Physical Sciences Research Council, the Science and Technology Facilities Council, and the Scottish Universities Physics Alliance; and the U.S. Department of Energy (DOE) and the National Science Foundation (NSF).

References

1. T. H. Bauer, R. D. Spital, D. R. Yenni and F. M. Pipkin, Rev. Mod. Phys. **50**, 261 (1978).
2. I. P. Ivanov, N. N. Nikolaev, A. A. Savin, Phys. Part. Nucl. **37**, 1 (2006).
3. K. Schilling, G. Wolf, Nucl. Phys. B **61**, 381 (1973).
4. H. Fraas, Ann. Phys. **87**, 417 (1974).
5. M. Diehl, JHEP **0709**, 064 (2007).
6. D. Müller et al., Fortschr. Phys. **42**, 101 (1994).
7. X. Ji, Phys. Rev. Lett. **78**, 610 (1997); Phys. Rev. D **55**, 7114 (1997).
8. A. V. Radyushkin, Phys. Rev. D **56**, 5524 (1997).
9. M. Diehl, Phys. Rep. **388**, 41 (2003).
10. A. V. Belitsky, A. V. Radyushkin, Phys. Rep. **418**, 1 (2005).
11. S. V. Goloskokov and P. Kroll, Eur. Phys. J. C **42**, 02298 (2005).
12. S. V. Goloskokov and P. Kroll, Eur. Phys. J. C **50**, 829 (2007).
13. S. V. Goloskokov and P. Kroll, Eur. Phys. J. C **53**, 367 (2008).
14. B. M. Vanderhaegen, P. A. M. Guichon, M. Guidal, Phys. Rev. Lett. **80**, 5064 (1998).

15. C. G. Goeke, M. V. Polyakov, M. Vanderhaegen, Prog. Part. Nucl. Phys. **47**, 401 (2001).
16. D. M. Guidal, M. V. Polyakov, A. V. Radyushkin, M. Vanderhaegen, Phys. Rev. **D72**, 054013 (2005).
17. J. C. Collins, L. Frankfurt and M. Strikman, Phys. Rev. D **56**, 2982 (1997).
18. A. Airapetian et al. (HERMES Collaboration), Eur. Phys. J. C **62**, 659 (2009).
19. S. Chekanov et al. (ZEUS Collaboration), PMC Phys. A **1**, 6 (2007).
20. F. D. Aaron et al. (H1 Collaboration), JHEP **1005**, 32 (2010).
21. M. Derrick et al. (ZEUS Collaboration), Phys. Lett. B **380**, 220 (1996).
22. J. Breitweg et al. (ZEUS Collaboration), Eur. Phys. J. C **6**, 603 (1999).
23. C. Adloff et al. (H1 Collaboration), Phys. Lett. B **483**, 360 (2000).
24. C. Adloff et al. (H1 Collaboration), Eur. Phys. J. C **13**, 371 (2000).
25. S. Aid et al. (H1 Collaboration), Nucl. Phys. B **468**, 3 (1996).
26. M. R. Adams et al. (E665 Collaboration), Z. Phys. C **74**, 237 (1997).
27. A. Airapetian et al. (HERMES Collaboration), Eur. Phys. J. C **17**, 389 (2000).
28. C. Hadjidakis et al. (CLAS Collaboration), Phys. Lett. B **605**, 256 (2005).
29. S. A. Morrow et al. (CLAS Collaboration), Eur. Phys. J. A **39**, 5 (2009).
30. D. Yu. Ivanov and R. Kirschner, Phys. Rev. D **58**, 114026 (1998).
31. E. V. Kuraev, N. N. Nikolaev, and B. G. Zakharov, Pis'ma ZHETF **68**, 667 (1998) (translation in JETP. Lett. **68**, 696 (1998)).
32. R. Kirschner, Nucl. Phys. B (Proc. Suppl.) **79**, 340 (1999).
33. N. Kivel, Phys. Rev. D **65**, 054010 (2002).
34. P. Joos et al., Nucl. Phys. B **113**, 53 (1976).
35. A. C. Irving, R. P. Worden, Phys. Rep. C **34**, 117 (1977).
36. G. L. Kane, A. Seidl. Rev. Mod. Phys. **48**, Part I, 309 (1976).
37. G. Cohen-Tannoudji, Ph. Salin, and A. Morel, Nuovo Cim. A **55**, 412 (1968).
38. M. N. Rosenbluth, Phys. Rev. **79**, 615 (1950).
39. J. Breitweg et al. (ZEUS Collaboration), Eur. Phys. J. C **12**, 393 (2000).
40. S. I. Manayenkov, Preprint PNPI 2856, Gatchina (2010).
41. K. Ackerstaff et al. (HERMES Collaboration), Nucl. Instr. and Meth. A **417**, 230 (1998).
42. A. Sokolov and I. Ternov, Sov. Phys. Doklady **8**, 1203 (1964).
43. D. P. Barber et al., Nucl. Instr. and Meth. A **329**, 79 (1993).
44. M. Beckmann et al. (HERMES Collaboration), Nucl. Instr. and Meth. A **479**, 334 (2002).
45. N. Akopov et al., Nucl. Instr. and Meth. A **479**, 511 (2002).
46. K. Ackerstaff et al. (HERMES Collaboration), Eur. Phys. J. C **18**, 303 (2000).
47. M. Tytgat, Ph.D. Thesis, Gent University, DESY-THESIS-2001-014 (2001).
48. A. A. Rostomyan, Ph.D. Thesis, Hamburg University, DESY-THESIS-2008-042 (2008).
49. CERN-CN Division, CERN Program Library Long Writeup D **506** (1992).
50. T. Sjöstrand, L. Lonnblad, S. Mrenna and P. Skands, PYTHIA 6.3: Physics and manual, hep-ph/0308153.
51. W. Augustyniak, A. Borissov, S. Manayenkov, arXiv:0808.0669 (2008).
52. S. V. Goloskokov, P. Kroll, Eur. Phys. J. C **59**, 809 (2009).
53. S.J. Brodsky, P. Hoyer, N. Marchal, S. Peigne and F. Sannino, Phys. Rev. D **65**, 114025 (2002).
54. B. Z. Kopeliovich, J. Nemchik and I. Schmidt, Phys. Rev. C **76**, 025210 (2007).
55. K. G. Boreskov, A. B. Kaidalov, O. V. Kancheli, Yad. Phys. **69**, 1802 (2006).

Appendix

A Systematic Uncertainty of the Amplitude Method for an Unpolarized Target

The systematic uncertainty arising from the neglect of amplitudes that make small contributions to the angular distribution applies if only data on unpolarized targets are considered. If the set of observables were enlarged and data on targets with transverse and longitudinal polarizations were added, then all the amplitude ratios could be extracted and there would be no contributory systematic uncertainty of the amplitude method.

The SDME analysis [18] of the HERMES data has shown the absence of any signal of the UPE amplitudes U_{01}, U_{10}, and U_{1-1}, violating the SCHC approximation. The contribution of the greatest UPE amplitude U_{11} to any SDME changes it by a value which is less or about one standard deviation of the statistical uncertainty. We neglect the contributions of U_{01}, U_{10}, and U_{1-1} to the SDMEs and do not consider that as a possible source of systematic uncertainty. The terms with the amplitudes U_{01}, U_{10}, and U_{1-1} in all the formulas considered in this appendix are also ignored. As explained in Sec. 4.2.1 the fractional contribution to SDMEs of NPE helicity-flip amplitudes are suppressed by α^2. The systematic uncertainty of the extracted amplitude ratios due to the neglect of the NPE nucleon helicity-flip amplitudes is the only uncertainty of the amplitude method which is considered below.

The true ratio of the NPE amplitude without helicity flip $T_{\lambda_V \frac{1}{2} \lambda_\gamma \frac{1}{2}}$ to $T_{0\frac{1}{2}0\frac{1}{2}}$ is denoted by $t_{\lambda_V\lambda_\gamma}$. The true ratio of the nucleon-helicity-flip amplitude $T^s_{\lambda_V\lambda_\gamma} \equiv T_{\lambda_V -\frac{1}{2}\lambda_\gamma \frac{1}{2}}$ to $T_{0\frac{1}{2}0\frac{1}{2}}$ is denoted by $t^s_{\lambda_V\lambda_\gamma}$, in particular, $t^s_{00} \equiv T_{0-\frac{1}{2}0\frac{1}{2}}$ $/T_{0\frac{1}{2}0\frac{1}{2}}$, while $|u_{11}|^2 \equiv (|U_{1\frac{1}{2}1\frac{1}{2}}|^2 + |U_{1-\frac{1}{2}1\frac{1}{2}}|^2)/|T_{0\frac{1}{2}0\frac{1}{2}}|^2$. In the following, we estimate the effect of neglecting small contributions of the NPE nucleon spin-flip amplitudes, $T^s_{\lambda_V\lambda_\gamma}$, which bias the fitted amplitude ratios by $\delta t_{\lambda_V\lambda_\gamma}$ and $\delta|u_{11}|$ respectively. In order to avoid misunderstandings, we note that the notation $t_{\lambda_V\lambda_\gamma}$ and $|u_{11}|$ in the main text was used for the fitted amplitude ratios which corresponds now to $t_{\lambda_V\lambda_\gamma} + \delta t_{\lambda_V\lambda_\gamma}$ and $|u_{11}| + \delta|u_{11}|$, respectively.

As shown in Eqs. (24-26), any SDME is multiplied by a function of the angles θ, Φ, ϕ and these functions are linearly independent. This means that every SDME (rather

than combinations of them) is determined in the fit individually. Now we assume that the true amplitude ratios are known, so that the true values of all SDMEs can be calculated.

The exact expression for r^{04}_{00}, which was presented in Ref. [18] and rewritten here in terms of the ratios of the helicity amplitudes $t_{\lambda_V\lambda_\gamma}$, $t^s_{\lambda_V\lambda_\gamma}$ and $|u_{11}|$, is

$$r^{04}_{00} = \frac{\epsilon(1+|t^s_{00}|^2)+|t_{01}|^2+|t^s_{01}|^2}{N_{tot}} \tag{A1}$$

where

$$\begin{aligned} N_{tot} &= \epsilon\Big(1+|t^s_{00}|^2+2|t_{10}|^2+2|t^s_{10}|^2\Big) \\ &+ |t_{11}|^2+|t^s_{11}|^2+|t_{01}|^2+|t^s_{01}|^2 \\ &+ |t_{1-1}|^2+|t^s_{1-1}|^2+|u_{11}|^2. \end{aligned} \tag{A2}$$

It is more convenient technically to consider a logarithm of r^{04}_{00}. The contribution to $\ln(r^{04}_{00})$ of the small NPE nucleon-helicity-flip amplitudes $|t^s_{00}|^2$, $|t^s_{10}|^2$, $|t^s_{11}|^2$, $|t^s_{01}|^2$ and $|t^s_{1-1}|^2$, linear in these small quantities, is

$$\begin{aligned} \Delta\ln(r^{04}_{00}) &= \Delta r^{04}_{00}/r^{04}_{00} = \frac{\epsilon|t^s_{00}|^2+|t^s_{01}|^2}{\epsilon+|t_{01}|^2} \\ &- \Big[\epsilon(|t^s_{00}|^2+2|t^s_{10}|^2)+|t^s_{11}|^2+|t^s_{01}|^2+|t^s_{1-1}|^2\Big] \\ &/\ \Big[\epsilon(1+2|t_{10}|^2)+|t_{11}|^2+|t_{01}|^2 \\ &+ |t_{1-1}|^2+|u_{11}|^2\Big]. \end{aligned} \tag{A3}$$

The formulas for r^{04}_{00} used in the fit of the angular distribution are

$$\widetilde{r}^{04}_{00} = \frac{\epsilon+|t_{01}|^2+\delta|t_{01}|^2}{\widetilde{N}_{tot}} \tag{A4}$$

where

$$\begin{aligned} \widetilde{N}_{tot} &= \epsilon\Big[1+2\Big(|t_{10}|^2+\delta|t_{10}|^2\Big)\Big] \\ &+ \Big(|t_{11}|^2+\delta|t_{11}|^2\Big)+\Big(|t_{01}|^2+\delta|t_{01}|^2\Big) \\ &+ \Big(|t_{1-1}|^2+\delta|t_{1-1}|^2\Big)+\Big(|u_{11}|^2+\delta|u_{11}|^2\Big) \end{aligned} \tag{A5}$$

with $\delta|t_{\lambda_V\lambda_\gamma}|^2 = t^*_{\lambda_V\lambda_\gamma}\delta t_{\lambda_V\lambda_\gamma} + t_{\lambda_V\lambda_\gamma}\delta t^*_{\lambda_V\lambda_\gamma}$ and $\delta|u_{11}|^2 = 2|u_{11}|\delta|u_{11}|$.

The contribution to $\ln(\widetilde{r}^{04}_{00})$ linear in the small quantities $\delta|t_{\lambda_V\lambda_\gamma}|^2$ and $\delta|u_{\lambda_V\lambda_\gamma}|^2$ is given by the relation

$$\begin{aligned} \delta\ln(\widetilde{r}^{04}_{00}) &= \frac{\delta\widetilde{r}^{04}_{00}}{\widetilde{r}^{04}_{00}} = \frac{\delta|t_{01}|^2}{\epsilon+|t_{01}|^2} \\ &- \Big[2\epsilon\delta|t_{10}|^2+\delta|t_{11}|^2+\delta|t_{01}|^2 \\ &+ \delta|t_{1-1}|^2+\delta|u_{11}|^2\Big] \\ &/\ \Big[\epsilon\Big(1+2|t_{10}|^2\Big)+|t_{11}|^2+|t_{01}|^2 \\ &+ |t_{1-1}|^2+|u_{11}|^2\Big]. \end{aligned} \tag{A6}$$

A comparison of Eqs. (A1) and (A2) with Eqs. (A4) and (A5) shows that $\widetilde{r}^{04}_{00} = r^{04}_{00}$ when $\delta t_{\lambda_V\lambda_\gamma} = \delta|u_{11}| = t^s_{\lambda_V\lambda_\gamma} = 0$. Since the fit has to reproduce the angular distribution, the contribution of the nucleon-helicity-flip amplitudes to r^{04}_{00} is compensated by the deviation of the obtained amplitude ratios from the true amplitude ratios. This assumes the validity of the relation

$$\Delta\ln(r^{04}_{00}) = \delta\ln(\widetilde{r}^{04}_{00}) \tag{A7}$$

which provides the linear relation between $|t^s_{\lambda_V\lambda_\gamma}|^2$ and $\delta|t_{\lambda_V\lambda_\gamma}|^2$, $\delta|u_{\lambda_V\lambda_\gamma}|^2$. Considering all other SDMEs $r^\eta_{\lambda_V\lambda'_V}$, use of the same method provides the set of relations for $\eta = 1-3,\ 5-8$

$$\Delta\ln(r^\eta_{\lambda_V\lambda'_V}) = \delta\ln(\widetilde{r}^\eta_{\lambda_V\lambda'_V}) \tag{A8}$$

which can be used to determine $\delta t_{\lambda_V\lambda_\gamma}$ and $\delta|u_{11}|$.

In order to get an approximate solution of Eq. (A7), the contributions of the s-channel helicity violating amplitudes T_{01}, T_{10}, and T_{1-1} (T^s_{01}, T^s_{10}, and T^s_{1-1}) are neglected since they are small compared to T_{00} and T_{11} (T^s_{00} and T^s_{11}). Putting Eqs. (A3) and (A6) into Eq. (A7) yields the relation

$$|t^s_{00}|^2 - \frac{\epsilon|t^s_{00}|^2+|t^s_{11}|^2}{\epsilon+|t_{11}|^2+|u_{11}|^2} = -\frac{\delta|t_{11}|^2+\delta|u_{11}|^2}{\epsilon+|t_{11}|^2+|u_{11}|^2}. \tag{A9}$$

Considering in the same way the matrix element r^1_{1-1} (or $\mathrm{Im}(r^2_{1-1})$) and using Eq. (A8) we get the relation

$$\begin{aligned} &\frac{|t^s_{11}|^2}{|t_{11}|^2-|u_{11}|^2} - \frac{\epsilon|t^s_{00}|^2+|t^s_{11}|^2}{\epsilon+|t_{11}|^2+|u_{11}|^2} \\ &= \frac{\delta|t_{11}|^2-\delta|u_{11}|^2}{|t_{11}|^2-|u_{11}|^2} - \frac{\delta|t_{11}|^2+\delta|u_{11}|^2}{\epsilon+|t_{11}|^2+|u_{11}|^2}. \end{aligned} \tag{A10}$$

The solution of the system of two equations (A9) and (A10) is

$$\delta|t_{11}|^2 = |t^s_{11}|^2 - |t^s_{00}|^2|t_{11}|^2, \tag{A11}$$

$$\delta|u_{11}|^2 = -|t^s_{00}|^2|u_{11}|^2. \tag{A12}$$

Dividing Eq. (A11) by $|t_{11}|^2$ and Eq. (A12) by $|u_{11}|^2$ these solutions can be rewritten for the fractional systematic uncertainties of $|t_{11}|^2$ and $|u_{11}|^2$ in the form

$$\frac{\delta|t_{11}|^2}{|t_{11}|^2} = \Big|\frac{T^s_{11}}{T_{11}}\Big|^2 - \Big|\frac{T^s_{00}}{T_{00}}\Big|^2, \tag{A13}$$

$$\frac{\delta|u_{11}|^2}{|u_{11}|^2} = 2\frac{\delta|u_{11}|}{|u_{11}|} = -|t^s_{00}|^2 \equiv -\Big|\frac{T^s_{00}}{T_{00}}\Big|^2. \tag{A14}$$

In order to obtain estimates for the real and imaginary parts of δt_{11}, we consider the SDMEs $\mathrm{Re}(r^5_{10})$ and $\mathrm{Re}(r^8_{10})$, respectively. The exact expression for $\mathrm{Re}(r^5_{10})$ taken from Ref. [18] and rewritten in terms of $t_{\lambda_V\lambda_\gamma}$, $t^s_{\lambda_V\lambda_\gamma}$, and $|u_{11}|$ is

$$\begin{aligned} \mathrm{Re}(r^5_{10}) = \frac{1}{\sqrt{8}}\mathrm{Re}\Big[&t_{11}-t_{1-1}+(t^s_{11}-t^s_{1-1})(t^s_{00})^* \\ &+ 2t_{10}(t_{01})^* + 2t^s_{10}(t^s_{01})^*\Big]/N_{tot} \end{aligned} \tag{A15}$$

where N_{tot} is defined by Eq. (A2). Using Eq. (A8) an approximate equation analogous to Eqs. (A9) and (A10) is obtained:

$$\frac{\mathrm{Re}[t^s_{11}(t^s_{00})^*]}{\mathrm{Re}(t_{11})} - \frac{\epsilon|t^s_{00}|^2 + |t^s_{11}|^2}{\epsilon + |t_{11}|^2 + |u_{11}|^2} = \frac{\mathrm{Re}(\delta t_{11})}{\mathrm{Re}(t_{11})} - \frac{\delta|t_{11}|^2 + \delta|u_{11}|^2}{\epsilon + |t_{11}|^2 + |u_{11}|^2}. \quad \text{(A16)}$$

Substituting into this equation the solutions for $\delta|t_{11}|^2$ and $\delta|u_{11}|^2$ given in Eqs. (A11) and (A12) leads to:

$$\mathrm{Re}(\delta t_{11}) = \mathrm{Re}[t^s_{11}(t^s_{00})^*] - |t^s_{00}|^2\mathrm{Re}(t_{11}). \quad \text{(A17)}$$

Considering $\mathrm{Re}(r^8_{10})$ analogously we get

$$\mathrm{Im}(\delta t_{11}) = \mathrm{Im}[t^s_{11}(t^s_{00})^*] - |t^s_{00}|^2\mathrm{Im}(t_{11}). \quad \text{(A18)}$$

Combining $\mathrm{Re}(\delta t_{11})$ and $\mathrm{Im}(\delta t_{11})$ into the complex number $\delta t_{11} = \mathrm{Re}(\delta t_{11}) + i \cdot \mathrm{Im}(\delta t_{11})$, the equation

$$\delta t_{11} = t^s_{11}(t^s_{00})^* - |t^s_{00}|^2 t_{11} \quad \text{(A19)}$$

is obtained which is equivalent to Eqs. (A17) and (A18). From Eq. (A19), it follows that

$$\frac{\delta t_{11}}{t_{11}} = \left(\frac{T^s_{11}}{T_{11}} - \frac{T^s_{00}}{T_{00}}\right)\left(\frac{T^s_{00}}{T_{00}}\right)^*. \quad \text{(A20)}$$

An analogous consideration of r^5_{00} and r^8_{00} provides the expression

$$\frac{\delta t_{01}}{t_{01}} = \left(\frac{T^s_{01}}{T_{01}} - \frac{T^s_{00}}{T_{00}}\right)\left(\frac{T^s_{00}}{T_{00}}\right)^*, \quad \text{(A21)}$$

while considering r^1_{11} and $\mathrm{Im}(r^3_{1-1})$ leads to:

$$\frac{\delta t_{1-1}}{t_{1-1}} = \left(\frac{T^s_{1-1}}{T_{1-1}} - \frac{T^s_{00}}{T_{00}}\right)\left(\frac{T^s_{11}}{T_{11}}\right)^*. \quad \text{(A22)}$$

Consideration of $\mathrm{Im}(r^6_{1-1})$ and $\mathrm{Im}(r^7_{1-1})$ leads to the relation

$$\frac{\delta t_{10}}{t_{10}} = \left(\frac{T^s_{10}}{T_{10}} - \frac{T^s_{00}}{T_{00}}\right)\left(\frac{T^s_{11}}{T_{11}}\right)^*. \quad \text{(A23)}$$

As shown in Ref. [40] the ratios of $T^s_{\lambda_V\lambda_\gamma}$ and $T_{\lambda_V\lambda_\gamma}$ obey the inequality

$$|T^s_{\lambda_V\lambda_\gamma}/T_{\lambda_V\lambda_\gamma}| \leq v_T/(2M), \quad \text{(A24)}$$

which gives the inequality

$$\left|\frac{T^s_{\lambda_V\lambda_\gamma}}{T_{\lambda_V\lambda_\gamma}} - \frac{T^s_{00}}{T_{00}}\right| \leq \left|\frac{T^s_{\lambda_V\lambda_\gamma}}{T_{\lambda_V\lambda_\gamma}}\right| + \left|\frac{T^s_{00}}{T_{00}}\right| \leq \frac{v_T}{M}. \quad \text{(A25)}$$

Inserting Eqs. (A24) and (A25) into expressions (A20-A23) yields the formulas of interest for the systematic uncertainty of $t_{\lambda_V\lambda_\gamma}$

$$|\delta t_{\lambda_V\lambda_\gamma}| \leq \frac{v_T^2}{2M^2}|t_{\lambda_V\lambda_\gamma}|. \quad \text{(A26)}$$

Since $|\mathrm{Re}(\delta t_{\lambda_V\lambda_\gamma})| \leq |\delta t_{\lambda_V\lambda_\gamma}|$ and $|\mathrm{Im}(\delta t_{\lambda_V\lambda_\gamma})| \leq |\delta t_{\lambda_V\lambda_\gamma}|$, the right hand side of relation (A26) can be used both for the real and imaginary parts of $\delta t_{\lambda_V\lambda_\gamma}$ yielding Eqs. (57) and (58). Relation (59) follows immediately from Eqs. (A14) and (A24).